



Article

Characterization of Virus-Inducible Orchid Argonaute 5b Promoter and Its Functional Characterization in *Nicotiana benthamiana* during Virus Infection

Kotapati Kasi Viswanath ^{1,†}, Song-Yi Kuo ^{1,†}, Ying-Wen Huang ^{1,2}, Nai-Wen Tsao ³, Chung-Chi Hu ^{1,2}, Na-Sheng Lin ⁴, Sheng-Yang Wang ³ and Yau-Heiu Hsu ^{1,2,*}

¹ Graduate Institute of Biotechnology, National Chung Hsing University, Taichung 40227, Taiwan

² Advanced Plant Biotechnology Center, National Chung Hsing University, Taichung 40227, Taiwan

³ Department of Forestry, National Chung Hsing University, Taichung 40227, Taiwan

⁴ Institute of Plant and Microbial Biology, Academia Sinica, Taipei 11529, Taiwan

* Correspondence: yhhsu@nchu.edu.tw

† These authors contributed equally to this work.



Citation: Kasi Viswanath, K.; Kuo, S.-Y.; Huang, Y.-W.; Tsao, N.-W.; Hu, C.-C.; Lin, N.-S.; Wang, S.-Y.; Hsu, Y.-H. Characterization of Virus-Inducible Orchid Argonaute 5b Promoter and Its Functional Characterization in *Nicotiana benthamiana* during Virus Infection. *Int. J. Mol. Sci.* **2022**, *23*, 9825. <https://doi.org/10.3390/ijms23179825>

Academic Editor:
Endang Septiningsih

Received: 22 June 2022

Accepted: 25 August 2022

Published: 29 August 2022

Publisher's Note: MDPI stays neutral with regard to jurisdictional claims in published maps and institutional affiliations.



Copyright: © 2022 by the authors. Licensee MDPI, Basel, Switzerland. This article is an open access article distributed under the terms and conditions of the Creative Commons Attribution (CC BY) license (<https://creativecommons.org/licenses/by/4.0/>).

Abstract: Plant ARGONAUTES (AGOs) play a significant role in the defense against viral infection. Previously, we have demonstrated that AGO5s encoded in *Phalaenopsis aphrodite* subsp. *formosana* (PaAGO5s) took an indispensable part in defense against major viruses. To understand the underlying defense mechanism, we cloned PaAGO5s promoters (*pPaAGO5s*) and analyzed their activity in transgenic *Nicotiana benthamiana* using β -glucuronidase (GUS) as a reporter gene. GUS activity analyses revealed that during *Cymbidium mosaic virus* (CymMV) and *Odontoglossum ringspot virus* (ORSV) infections, *pPaAGO5b* activity was significantly increased compared to *pPaAGO5a* and *pPaAGO5c*. Analysis of *pPaAGO5b* 5'-deletion revealed that *pPaAGO5b_941* has higher activity during virus infection. Further, yeast one-hybrid analysis showed that the transcription factor NbMYB30 physically interacted with *pPaAGO5b_941* to enhance its activity. Overexpression and silencing of *NbMYB30* resulted in up- and downregulation of *GUS* expression, respectively. Exogenous application and endogenous measurement of phytohormones have shown that methyl jasmonate and salicylic acid respond to viral infections. NbMYB30 overexpression and its closest related protein, PaMYB30, in *P. aphrodite* subsp. *formosana* reduced CymMV accumulation in *P. aphrodite* subsp. *formosana*. Based on these discoveries, this study uncovers the interaction between virus-responsive promoter and the corresponding transcription factor in plants.

Keywords: Argonautes 5b; CymMV; ORSV; MeJA; NbMYB30; SA

1. Introduction

Emerging plant viruses and their pathogenicity are major issues in plant virology [1]. RNA silencing is considered to be an important mechanism to help plants fight against viruses [2,3]. The siRNA from virus or miRNA from host is loaded into the RAN-induced silencing complex (RISC). The binding preference of argonaute proteins to small RNA determines the small RNA species that can be loaded into RISC. With the proper combination of small RNA and AGO proteins, RISC can be led to designated targets to regulate or participate in the defense system against viruses [4,5].

Accumulating evidence indicates that several plant AGOs have antiviral functions. For example, the potential antiviral activities of AtAGO1 and AtAGO7 against *Turnip crinkle virus* (TCV) mutants [6], AtAGO2 and AtAGO5 against *Potexvirus X* (PVX) [7], and AtAGO2 and AtAGO3 against *Bamboo mosaic virus* (BaMV) infection have been reported in *Arabidopsis* [8]. In rice, OsAGO1 and OsAGO18 exhibit antiviral activity against the *Rice stripe virus* (RSV) and *Rice dwarf virus* (RDV) [9]. In *Nicotiana benthamiana*, NbAGO1 and NbAGO2 show antiviral activity against *Tomato ringspot virus* (ToRSV), *Tomato bushy*

stunt virus (TBSV) P19 suppressor mutants [10,11], and *Tobacco mosaic virus* (TMV) [12]. *N. benthamiana* AGO4 is involved in PVX resistance [13], and NbAGO5 is also able to bind *Cucumber mosaic virus* (CMV) vsRNAs [14], signifying its role in antiviral defense. Our previous study identified that NbAGO1-restricted BaMV and NbAGO10 might compete with NbAGO1 for BaMV-derived small interfering RNAs (vsRNAs) to protect BaMV from NbAGO1-mediated antiviral RNA silencing in *N. benthamiana* [15].

Plant hormones, such as salicylic acid (SA), jasmonic acid (JA), and abscisic acid (ABA), play a crucial role in regulating the defense mechanism against pathogen infection [16]. In addition, increasing evidence has shown the role of phytohormones as mediators of RNA silencing [17,18]. For example, ABA induces resistance to PVX and BaMV [8] by regulating AtAGO2 and AtAGO3 in *Arabidopsis*. NbAGO2 was transcriptionally induced by methyl salicylate treatment and TMV infection in *N. benthamiana* [12]. In *Arabidopsis*, treatment with SA and ABA together slightly increased the expression of AtAGO2, whereas ABA treatment alone increased the expression of AtAGO4, AtAGO6, and AtAGO7 [19]. The transcriptional activity of AtAGO1 and OsAGO18 has been shown to increase during ABA [20] and JA treatment [21], respectively. In addition to phytohormones, the transcriptional regulation of stress-responsive genes through binding transcription factors (TFs) is an essential part of the plant response to viral infection. Various TFs, including NAC (NAM, ATAF1,2 and CUC2) [22–24], MYB (myeloblastosis related) [24–26], AP2/ERF (APETALA2/ethylene-responsive factor) [27], WRKY [28], and bZIP (basic leucine zipper) [29,30] are involved in viral stress responses.

Orchids have a unique status in floricultural crops that are commercially grown worldwide. The moth orchid, *P. aphrodite* subsp. *formosana* is renowned for its extraordinary floral diversity, implying complex flower color development, and is one of the most valuable research materials for molecular biology studies [31]. However, the farming and marketability of orchids have been seriously hampered by various pathogens, specifically viruses, which are not efficiently controlled by pesticide applications [32]. Two major infectious viruses of orchids, *Cymbidium mosaic virus* (CymMV) and *Odontoglossum ringspot virus* (ORSV), pose severe threats to the orchid industry. Recently, we identified that the *P. aphrodite* subsp. *formosana* AGO5 (PaAGO5) protein family plays a vital role in defense against CymMV and ORSV [33]. Specifically, PaAGO5b enhances resistance against CymMV and ORSV. More recently, we explored the induced activity of TF NbNAC42 on NbAGO5 under BaMV infection in *N. benthamiana* (provisionally accepted). To date, little is known about the effect of viral infection on the AGO gene promoters. Moreover, the extent to which TFs and phytohormones affect the expression and function of AGOs during viral infections remains to be determined.

To uncover the inducing effect of the viruses on the AGO promoter, we selected the PaAGO5b promoter for the current study because of the significant upregulation of PaAGO5b transcripts during CymMV and ORSV infection. Hence, the objective of this study was to identify the factors that activate PaAGO5b expression by exploring PaAGO5b promoter activity in transgenic *N. benthamiana*.

2. Results

2.1. Identification and In Silico Analysis of PaAGO5 Promoters

We cloned and sequenced *P. aphrodite* subsp. *formosana* AGO5a, AGO5b, and AGO5c putative promoter sequences with 2759-, 2029-, and 2589-bp lengths. TSS and the 5'-UTR were identified (Supplementary Figure S1). A BLAST search revealed that *P. aphrodite* subsp. *formosana* AGO5a, AGO5b, and AGO5c promoter sequences showed 95.23%, 99.74%, and 98.98% identity with those of *P. equestris*. The cloned promoter sequences were named *pPaAGO5a*, *pPaAGO5b*, and *pPaAGO5c* (*p*-indicates promoter) and analyzed using PlantCARE to identify possible *cis*-acting elements. We found numerous *cis*-acting elements connected to plant growth and development, phytohormone responses, and stress responses, including core transcriptional regulatory elements (i.e., TATA-box and CAAT-box) (Supplementary Tables S1–S3).

2.2. Activity of *pPaAGO5s* in *P. aphrodite* subsp. *formosana* and *N. benthamiana* during CymMV and ORSV Infection

To characterize the promoter activities, GUS was used as a reporter in the following experiments. Recombinant constructs *pCAMBIA-pPaAGO5a::GUS*, *pCAMBIA-pPaAGO5b::GUS*, and *pCAMBIA-pPaAGO5c::GUS* (Supplementary Figure S2) were agroinfiltrated for transient expression in WT *P. aphrodite* subsp. *formosana* and *N. benthamiana*. At 3 dpi, leaves were detached to check for GUS activity. Histochemical staining data from *P. aphrodite* subsp. *formosana* showed visible accumulation of blue dye in *pPaAGO5b* leaf discs and low and basal activity levels in *pPaAGO5a* and *pPaAGO5c* leaf discs without CymMV or ORSV infection (Supplementary Figure S3). However, during CymMV or ORSV infection, the blue color intensity was higher in the leaf discs of *pPaAGO5b* than in *pPaAGO5a* and *pPaAGO5c* (Supplementary Figure S3). The histochemical results were further validated by fluorometric quantification of GUS activity. Among the three promoters, *pPaAGO5b* showed the highest activity in *P. aphrodite* subsp. *formosana* (Figure 1A) and *N. benthamiana* (Figure 1B). Particularly, after CymMV and ORSV infection, *pPaAGO5b* activity was significantly enhanced in *P. aphrodite* subsp. *formosana* and *N. benthamiana* leaves compared with no viral infection (Figure 1A,B). GUS activity levels were not detected in the mock treatment (infiltration with buffer only), negative control, or empty vector (EV; pKn). GUS activity results in *P. aphrodite* subsp. *formosana* and *N. benthamiana* revealed that only *pPaAGO5b* was induced during CymMV and ORSV infection.

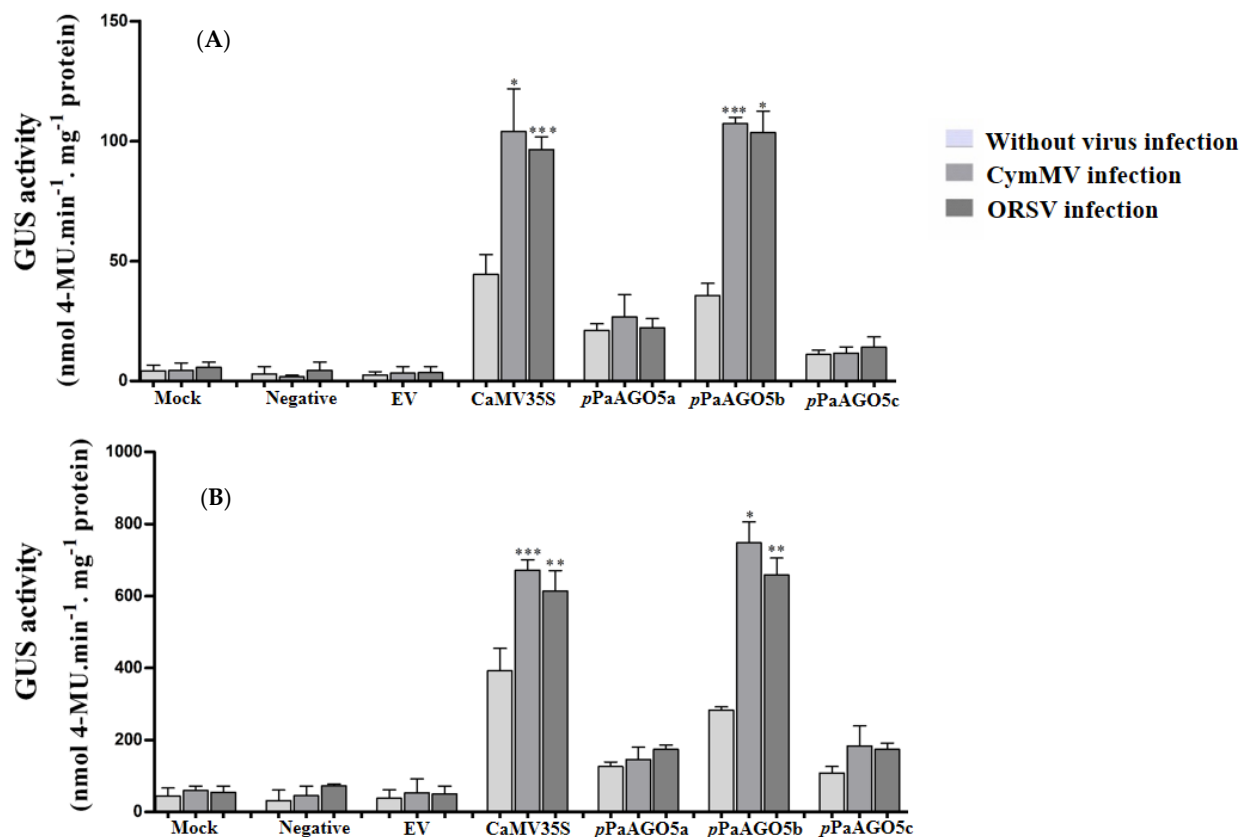


Figure 1. GUS fluorescent quantitative analysis of the *pPaAGO5a*, *pPaAGO5b*, and *pPaAGO5c*. The GUS activity in the wild-type (A) *P. aphrodite* subsp. *formosana* and (B) *N. benthamiana* leaves during CymMV and ORSV infection at 3 days post-inoculation (dpi). Each promoter GUS construct was assayed at least three times in four independent experiments. The GUS activity, 4-MU nmol-produced min⁻¹ mg⁻¹ protein, is represented as the mean \pm SD of each mock (infiltration buffer only), negative and empty vector (EV; pKn), CaMV 35S, *pPaAGO5a*, *pPaAGO5b*, and *pPaAGO5c*. Data are mean \pm SD, * $p < 0.05$, ** $p < 0.01$, *** $p < 0.001$ by Student's *t*-test, respectively.

2.3. Detection of *pPaAGO5b* Activity during Various Virus Infections and Viral Gene Expression in Transgenic *N. benthamiana*

Based on the preliminary GUS activity data (Figure 1A,B), we selected *pPaAGO5b* for further characterization. To investigate the strength of *pPaAGO5b*, infectious clones of various viruses were agroinfiltrated into transgenic *N. benthamiana* leaves harboring the reporter construct, pCAMBIA-*pPaAGO5b*::GUS. Before agroinfiltration, the T₃ progeny per construct was confirmed by PCR to detect the presence of *GUS* and *HygR* (Supplementary Figure S4). We also explored tissue-specific GUS expression in transgenic *N. benthamiana* during the developmental stages by histochemical staining (Figure 2). Seeds, germinated seedlings, leaves, stems, roots, flowers, and anthers were collected from each line. According to the staining results (Figure 2), constitutive expression of GUS was observed in the *pPaAGO5b* transgenic line compared to those in *pPaAGO5a* and *pPaAGO5c*. In contrast, GUS activity was undetectable in the healthy plants and negative controls (Figure 2). These results indicate that PaAGO5b may play a significant role in plant growth and development.

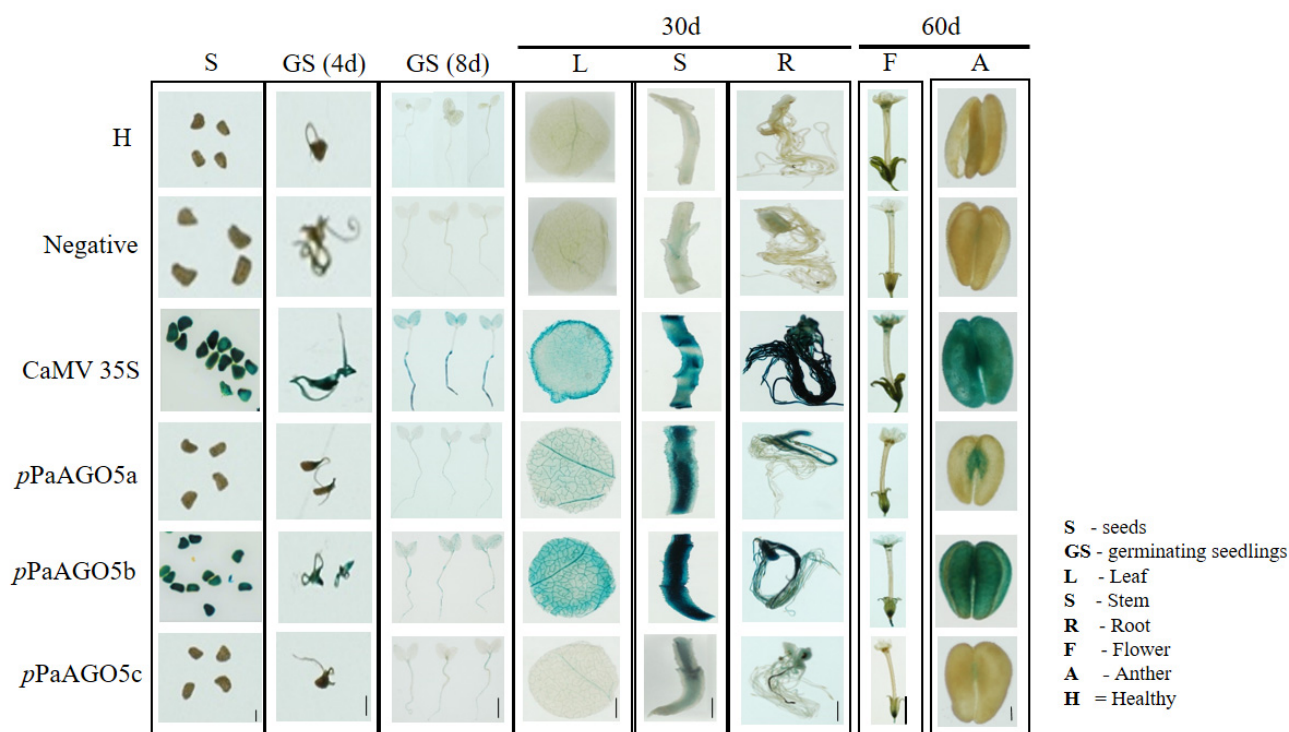


Figure 2. GUS histochemical staining in tissues of transgenic *N. benthamiana*. GUS expression driven by *pPaAGO5a*, *pPaAGO5b*, *pPaAGO5c*, CaMV 35S, and negative constructs. H represents healthy plants. As per the staining analysis, in CaMV 35S transgenic line, constitutive expression of GUS was observed in seeds, germinating seedlings, leaf, stem, root, flower, and anther. In the *pPaAGO5a* transgenic line, low expression of GUS was observed in germinating seedling, leaf, flower, and anther, moderate expression was observed in stem and root, and no expression was observed in seeds. In the *pPaAGO5b* transgenic line, higher expression of GUS expression was noticed in seeds, germinating seedlings, leaf, stem, root, flower, and anther. In the *pPaAGO5c* transgenic line, extremely low expression in germinating seedlings, leaf, and anther, low expression in the stem and root, and no expression in seeds have been observed. GUS activity was undetectable in healthy plants (H) and negative controls. The seeds, 4- and 8-day-old germinating seedlings, leaves, roots, stems of 30-day-old plants, and flowers and anthers of 60-day-old plants were incubated in GUS staining solution at 37 °C for 12 h. Scale bar of seeds: 0.1 cm; scale bar of anthers: 0.2 cm; the other scale bars: 1 cm.

After confirming tissue-specific expression in T₃ progeny, we quantified the GUS activity level driven by *pPaAGO5b* during CymMV and ORSV infection. As per GUS

quantification, *pPaAGO5b* activity was significantly enhanced by 3.5-fold and 2.5-fold, respectively, compared to that without CymMV and ORSV infection (leaves infiltrated only with EV) (Figure 3A). To evaluate the compatibility of *pPaAGO5b*, we inoculated BaMV, PVX, TMV, and FoMV infectious clones into transgenic *N. benthamiana* leaves. GUS quantitative fluorescence results at 3 dpi showed that *pPaAGO5b* significantly increased the GUS activity during the infections of BaMV (2.5-fold), TMV (1.5-fold), and FoMV (2.5-fold), but not PVX (Figure 3A). In contrast, the GUS activity driven by *pPaAGO5a* and *pPaAGO5c* did not differ from those of CymMV, ORSV, BaMV, PVX, TMV, and FoMV (Supplementary Figure S5). Furthermore, GUS activity was not detected in negative controls (Figure 3A). These results suggest that, except for PVX, the remaining infiltrated virus infectious clones had an inducing effect on *pPaAGO5b*. However, we did not observe the inducing effect of PVX not only in the infiltration site but also in systemic leaves at 10 dpi (data not shown).

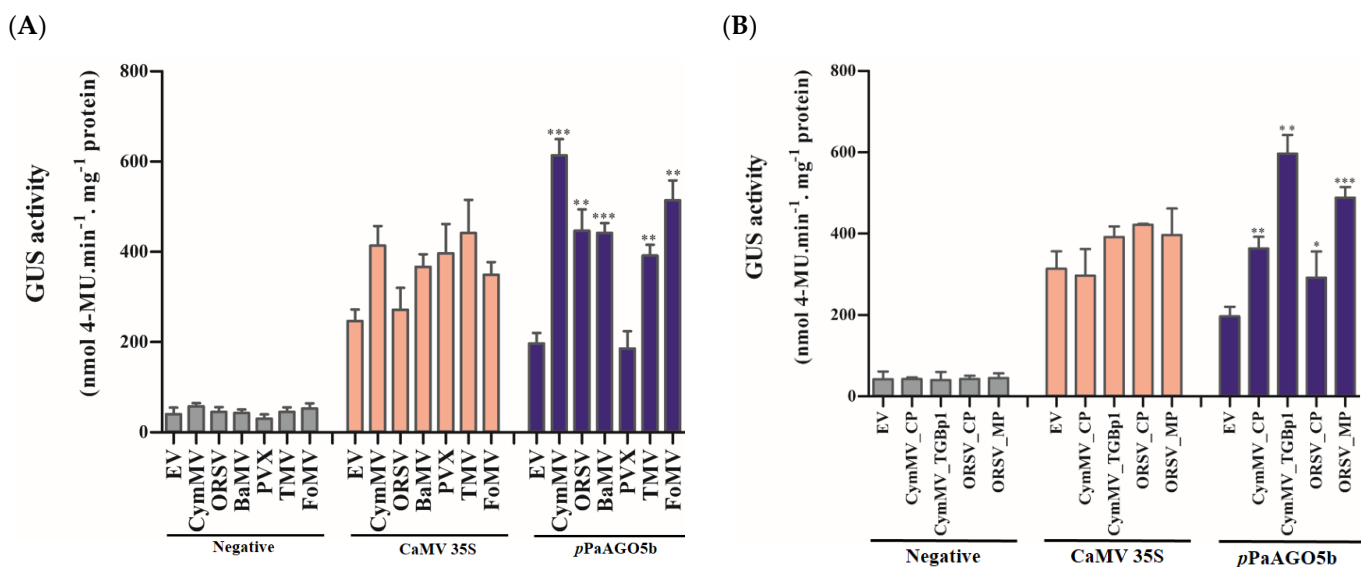


Figure 3. GUS fluorescent quantitative activity of *pPaAGO5b* during virus infection and expression of viral genes. (A) GUS fluorescent quantitative analysis of the negative CaMV 35S and *pPaAGO5b* during CymMV, ORSV, BaMV, PVX, TMV, and FoMV infection in transgenic *N. benthamiana* leaves at 3 dpi. (B) GUS fluorescent quantitative analysis of the negative CaMV 35S and *pPaAGO5b* during CymMV_CP, CymMV_TGBp1, ORSV_CP, and ORSV_MP overexpression in transgenic *N. benthamiana* leaves at 3 dpi. Each promoter GUS construct was assayed at least three times in four independent experiments. The GUS activity, 4-MU nmol-produced min⁻¹ mg⁻¹ protein, is represented as the mean \pm SD of each negative control, CaMV 35S, *pPaAGO5b*. Data are mean \pm SD, * $p < 0.05$, ** $p < 0.01$, *** $p < 0.001$ by Student's *t*-test, respectively.

To determine the viral proteins involved in regulating *pPaAGO5b* activity, we infiltrated CymMV_CP, CymMV_TGBp1, ORSV_CP, and ORSV_MP overexpression constructs (Supplementary Figure S6) into transgenic *N. benthamiana* leaves. As a result, the *pPaAGO5b* activity was increased by 2-, 3.5-, 1-, and 2.5-fold with CymMV_CP, CymMV_TGBp1, ORSV_CP, and ORSV_MP overexpression, respectively, compared to those without viral gene expression (leaves infiltrated only with EV) (Figure 3B). However, *pPaAGO5a* and *pPaAGO5c* expressions were not significantly enhanced by the viral proteins we tested, as described (Supplementary Figure S7). In parallel, GUS activity was not detected in the negative controls (Figure 3B). These results suggest that CymMV_TGBp1 and ORSV_MP had a greater effect on *pPaAGO5b*.

2.4. Mapping of *pPaAGO5b* (Virus-Responsive Element) by Using 5'-Deletion Constructs in *N. benthamiana* during CymMV and ORSV Infection or Viral Gene Expression

The *pPaAGO5b* showed significantly increased activity during viral infection and the overexpression of viral genes (Figure 3A,B). To determine which region of *pPaAGO5b* determines activity levels during viral infection, we functionally investigated the 5'-deletion constructs of *pPaAGO5b* based on *cis*-acting elements, which play a role during stress conditions. A total of ten 5'-truncated *pPaAGO5b* fragments of different sizes (−1782, −1582, −1182, −941, −582, −349, −235, −109, −88, and −65 bp upstream to TSS) were amplified from the *pPaAGO5b* full-length promoter. Each construct was co-infiltrated with CymMV or ORSV infectious clones or viral genes. The results of the 5'-deletion transient assay in *N. benthamiana* are shown in Figure 4. During CymMV infection (Figure 4A) or overexpression of CymMV_CP (Figure 4B) or CymMV_TGBp1 (Figure 4C), *pPaAGO5b_941* exhibited maximal activity, followed by *pPaAGO5b_full-length*, *pPaAGO5b_1782*, *pPaAGO5b_1582* as compared to those without CymMV infection or the expression of CymMV_CP or CymMV_TGBp1. During ORSV infection (Figure 4D) or overexpression of ORSV_CP (Figure 4E), ORSV_MP (Figure 4F) and *pPaAGO5b_941* exhibited maximal activity, followed by *pPaAGO5b_full-length*, *pPaAGO5b_1782*, and *pPaAGO5b_1582* as compared to those without ORSV infection or ORSV_CP or ORSV_MP. The 5'-deletion constructs *pPaAGO5b_582*, *pPaAGO5b_349*, *pPaAGO5b_109*, *pPaAGO5b_88*, and *pPaAGO5b_65* (UTR alone) exhibited relatively poor activity compared with the remaining 5'-deletion constructs (Figure 4A–F). GUS activity levels were not detected in mock, EV, or negative control treatments.

2.5. Quantitative Analysis of TFs during Virus Infection and Yeast One-Hybrid Analysis

To examine the expression profiles of selected TFs identified in the *in silico* analysis (NbMYB94, NbREV8, NbLHY, NbMYB30, and NbCIR1), transgenic *N. benthamiana* leaves were infiltrated with CymMV infectious clones. The plants were kept at 25 °C with a 16 h light period, and leaf samples were collected at 72 h post infiltration (hpi). The real-time qRT-PCR results showed that among the five TFs, NbMYB30 and NbREV8 activity was significantly upregulated after CymMV infection compared with EV (pKn) infiltration (Supplementary Figure S8). Likewise, we analyzed the expression profile of TFs NbNAC42 and NbZFP3 and proved activator and repressor of NbAGO5 in *N. benthamiana*. The real-time qRT-PCR results showed that both NbNAC42 and NbZFP3 did not exhibit enhancement in activity (Supplementary Figure S8).

To test whether the enhanced activity of *pPaAGO5b* was due to the direct effect of viral genes or an indirect effect through the interaction of TFs, we selected *pPaAGO5b_941* and performed the Y1H assay. Based on the Y1H analysis, we did not find an interaction between *pPaAGO5b_941* and viral genes such as CymMV_CP, CymMV_TGBp1, ORSV_CP, and ORSV_MP on SD/−Leu/−Trp/−His plates supplemented with 20 mM 3-AT (Figure 5A). Furthermore, we performed Y1H assay to examine the interaction between *pPaAGO5b_941* and TFs. Among the five TFs (NbMYB94, NbREV8, NbLHY, NbMYB30, and NbCIR1), we observed the growth of *pPaAGO5b_941* and NbMYB30 containing Y187 cells on SD/−Leu/−Trp/−His plates supplemented with 20 mM of 3-AT (Figure 5A). Therefore, we found that the enhanced activity of *pPaAGO5b_941* during viral infection is indirect, indicating that virus infection could upregulate TF NbMYB30 and interact with the promoter region *pPaAGO5b_941*. We did not observe any physical interactions in the negative controls (Figure 5B).

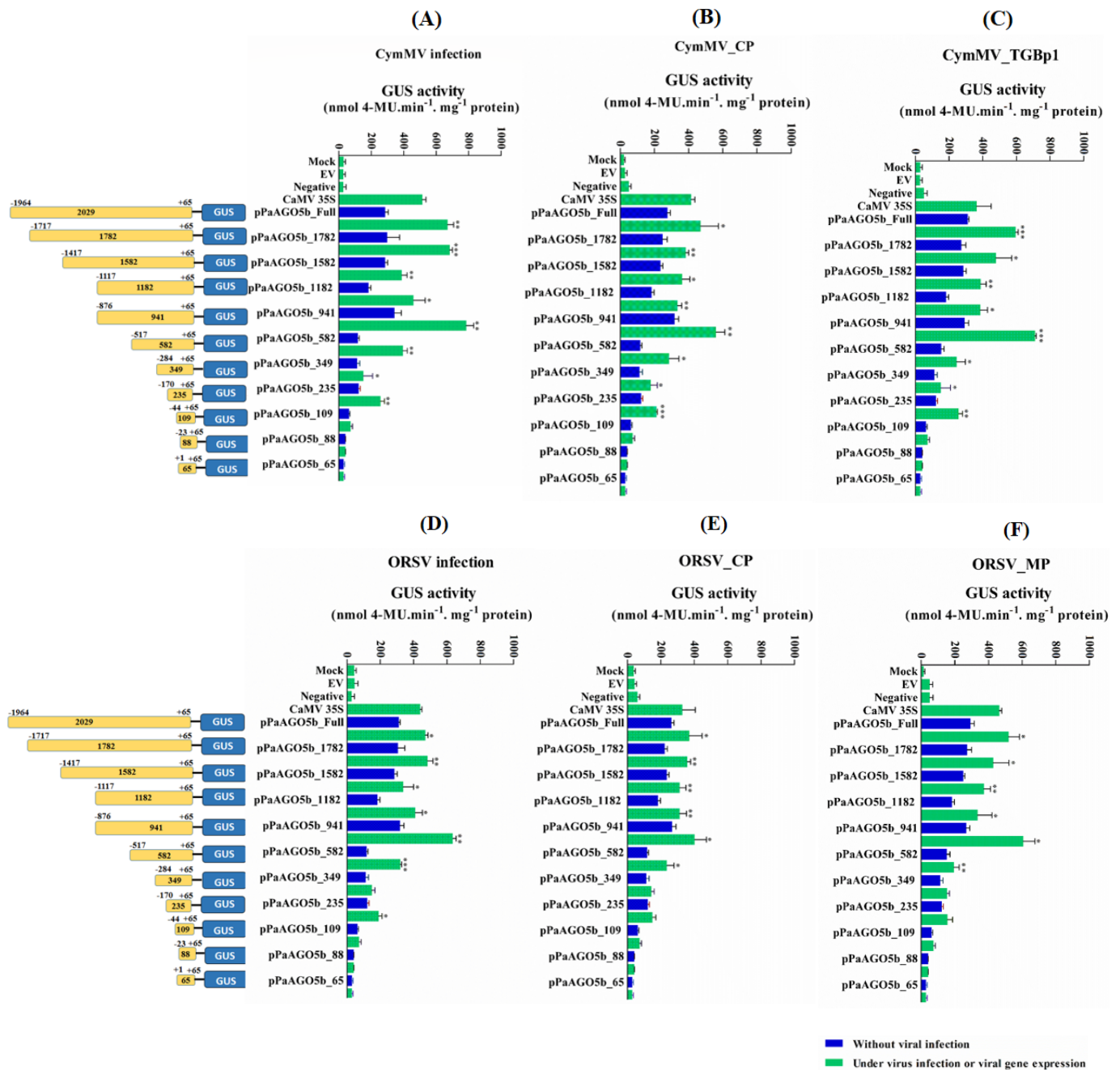


Figure 4. GUS fluorescent quantitative analysis of the 5'-deletion constructs of *pPaAGO5b*. The activity level of *pPaAGO5b* 5'-deletion constructs during (A) CymMV infection, (B) CymMV_CP, overexpression, (C) CymMV_TGBp1 overexpression, (D) ORSV infection, (E) ORSV_CP, and (F) ORSV_MP overexpression in wild-type *N. benthamiana* leaves at 3 dpi. Each 5'-deletion promoter construct (mentioned in the figure with length) was assayed at least three times in four independent experiments. The GUS activity, 4-MU nmol-produced min⁻¹ mg⁻¹ protein, is represented as the mean ± SD of each mock, empty vector (EV; pKn for the CymMV and ORSV infection; pEPYON-32K for the viral genes expression analysis), negative control and CaMV 35S, and 5'-deletion promoter GUS constructs. Data are mean ± SD, * *p* < 0.05, ** *p* < 0.01, *** *p* < 0.001 by Student *t*-test, respectively.

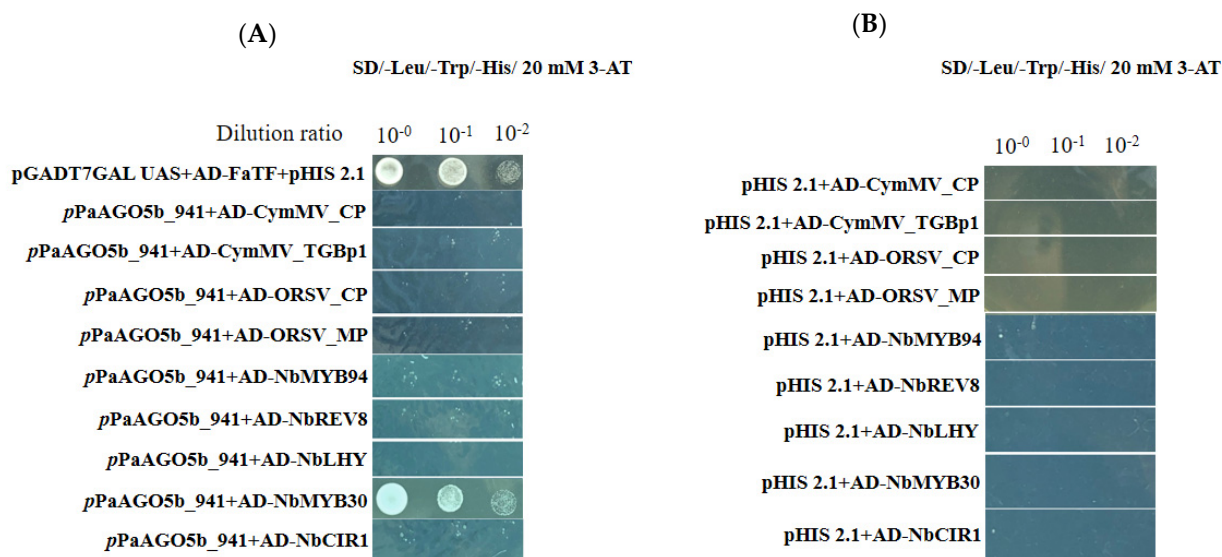


Figure 5. Physical interaction between *pPaAGO5b_941* and viral genes or TFs in yeast cells. The full-length clones of CymMV_CP, CymMV_TGBp1, ORSV_CP, ORSV_MP, NbMYB94, NbREV8, NbLHY, NbMYB30, and NbCIR1 and were fused to pGADT74-AD and *pPaAGO5b_941* fused to pHIS 2.1-BD were cotransformed and expressed in the yeast strain Y187. The transformed yeast cells were grown in non-selective media with histidine (SD/-Leu/-Trp) (Supplementary Figure S14) or (A) selective media without histidine with 20 mM 3-AT (SD/-Leu/-Trp/-His), followed by incubation at 30 °C for 3 days. The pHIS 2.1 vector and pGADT74-AD cotransformed with strawberry heat shock TF (FaTF) fused with pGBKT7 vector into yeast cells were used as the positive control. (B) The pHIS 2.1 vector and cotransformed with CymMV_CP, CymMV_TGBp1, ORSV_CP, ORSV_MP, NbMYB94, NbREV8, NbLHY, NbMYB30, and NbCIR1 into yeast cells were used as the negative controls.

2.6. Effect of NbMYB30 on GUS Expression Driven by the *pPaAGO5b* in *N. benthamiana*

To validate the effect of NbMYB30 on *GUS* expression, driven by the *pPaAGO5b*, we performed the overexpression and TRV-based silencing experiments in transgenic *N. benthamiana* with pCAMBIA-*pPaAGO5_941::GUS*. To overexpress NbMYB30, the coding region of NbMYB30 was amplified with a FLAG-tag, and its expression was confirmed by Western blotting (Supplementary Figure S9). After confirming the expression of NbMYB30, 28-day-old *N. benthamiana* leaves were agroinfiltrated with *A. tumefaciens* strain GV3850 cells harboring pEPFlag-NbMYB30. For analysis, the leaves were sampled at 1, 2, and 3 dpi. In addition, the expression level of *GUS* was analyzed by real-time qRT-PCR and *GUS* fluorometric analysis. The mRNA expression profile of *GUS* significantly increased during the overexpression of NbMYB30 compared with those infiltrated with EV (Figure 6A). Similar findings were observed through *GUS* fluorimetric analysis (Figure 6B).

For loss-of-function experiment, NbMYB30 expression was transiently knocked down using TRV-based VIGS. Plants infiltrated with the luciferase-silencing (Luci) construct were used as the negative control. Real-time qRT-PCR analysis displayed that the transcription of NbMYB30 was specifically downregulated to 0.03-fold of that of the negative control at 10 dpi (Figure 6C). Furthermore, the expression level of *GUS* during NbMYB30 knockdown decreased to 0.52-fold compared to that of the negative control (Figure 6C). The results of the overexpression and silencing analyses further support the assumption that *PaAGO5b* expression is positively associated with NbMYB30.

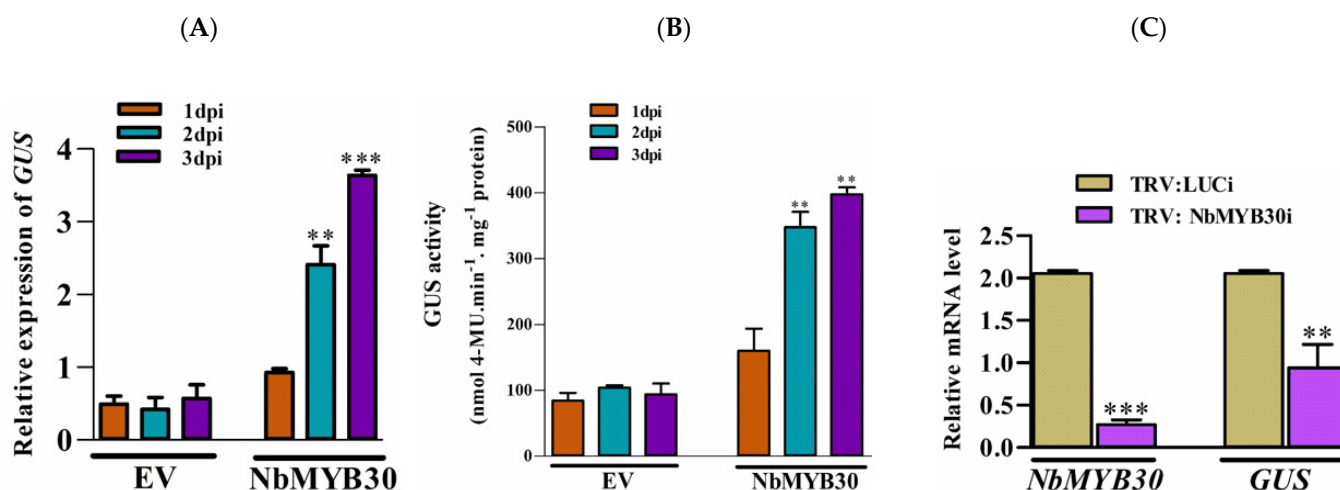


Figure 6. Effects of overexpression and silencing of NbMYB30 on *GUS* transcript levels in transgenic *N. benthamiana* plants. (A) The expression level of *GUS* was analyzed by real-time qRT-PCR, and (B) the activity level of *GUS* was analyzed by fluorimetric analysis. The transient expression effect of NbMYB30 significantly enhanced the *GUS* expression and activity level. (C) The TRV-based silencing of *NbMYB30* significantly downregulated the transcript level *GUS* in transgenic *N. benthamiana* plants. Data are mean \pm SD, ** $p < 0.01$, *** $p < 0.001$ by Student *t*-test, respectively.

2.7. Responses of NbMYB30 on Challenges of CymMV and ORSV in *N. benthamiana*

To validate the effect of CymMV or ORSV infectious clones and viral genes on the expression of *NbMYB30*, we co-infiltrated the transgenic *N. benthamiana* plants with the pCAMBIA-*pPaAGO5_941::GUS* construct with infectious clones of CymMV, ORSV, and transient expression construct of viral genes. Real-time qRT-PCR expression profiles revealed that *NbMYB30* expression was significantly increased following the challenge with CymMV and ORSV, and expression of CymMV_CP, CymMV_TGBp1, ORSV_CP, and ORSV_MP compared with that in the EV-treated control plants (Supplementary Figure S10). These findings support that endogenous *NbMYB30* significantly responded to viral infection and enhanced the activity levels.

2.8. The Response of *pPaAGO5b* to Phytohormone Treatments

Phytohormones, such as SA, JA, and ABA, play key roles during biotic stress. Various phytohormone-responsive elements were recognized in the promoter sequence of *pPaAGO5b* (Supplementary Table S2), indicating that *pPaAGO5b* may affect various phytohormone-related metabolic activities that regulate plant growth and development during pathogen infection. To evaluate the effect of phytohormones on *pPaAGO5b*, 1 mM SA, 100 μ M MeJA, and 100 μ M ABA were sprayed exogenously on transgenic *N. benthamiana* leaves. *GUS* fluorometric assays showed that *GUS* expression was significantly induced by SA (Figure 7A) and MeJA (Figure 7B) at 72 h, but not by ABA (Figure 7C) treatment. Furthermore, we examined the *GUS* activity levels with a combination of phytohormones and CymMV or ORSV infection at 72 h. According to *GUS* fluorimetric analysis, with the combination of virus infection and 1 mM SA or 100 μ M ABA treatment, no significant increase was noted compared with CymMV and ORSV infection or hormone treatment alone (Figure 7A,C). However, *pPaAGO5b* activity significantly increased with the combination of CymMV or ORSV infection with 100 μ M MeJA, compared with CymMV or ORSV infection or hormone alone (Figure 7B). These results indicate that SA and MeJA induced *GUS* driven by *pPaAGO5b*. Furthermore, the combination of virus infection and MeJA significantly induced *GUS*, specifying that MeJA might act as a major inducing hormone during CymMV or ORSV infection. This requires further investigation.

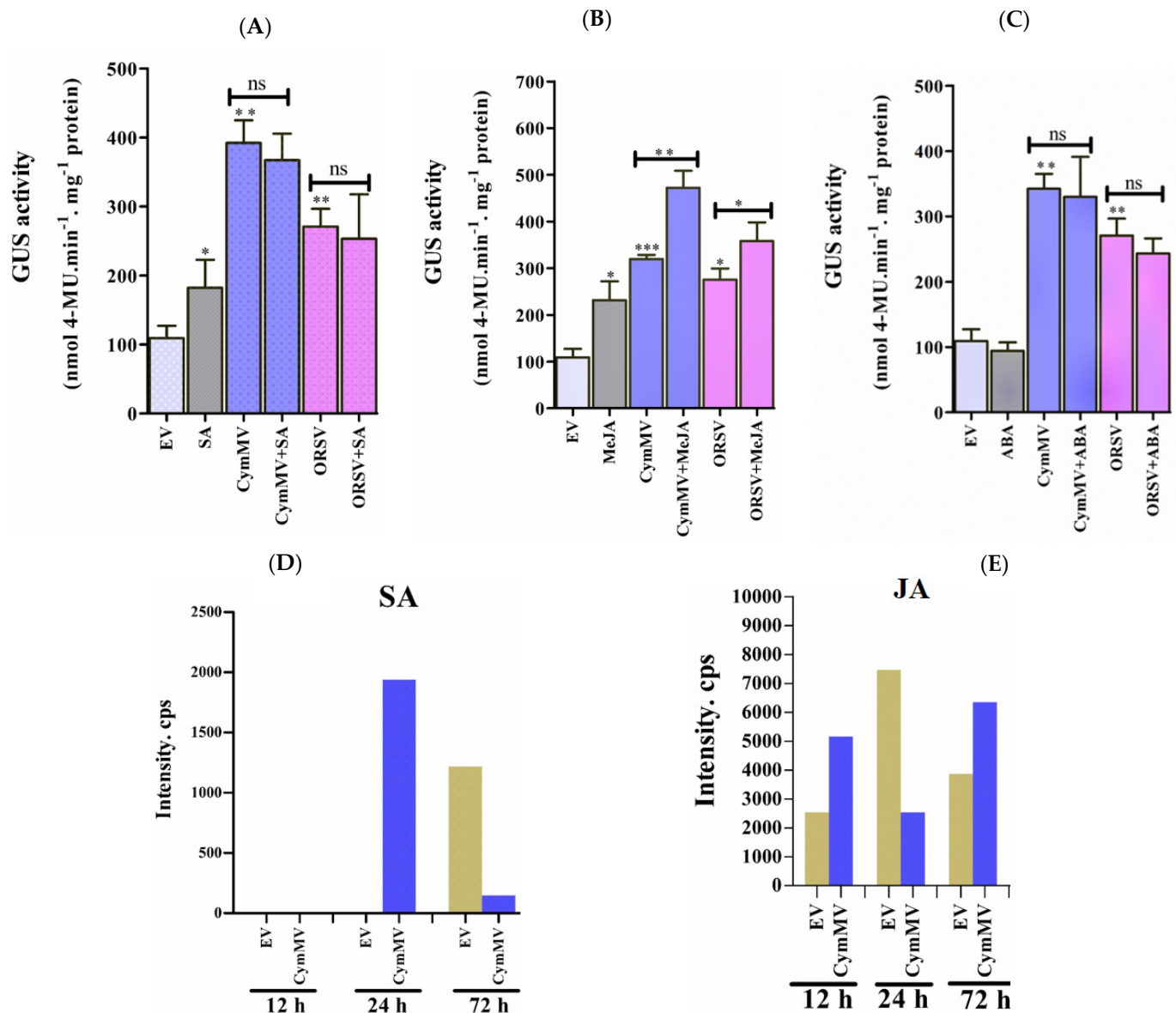


Figure 7. GUS fluorescent quantitative analysis during exogenous application of phytohormones and measurement of endogenous SA and JA levels. The activity of GUS driven by the *pPaAGO5b* measured during exogenous application of (A) 1 mM SA, (B) 100 μ M MeJA, and (C) 100 μ M ABA treatment alone or virus infection alone or a combination of phytohormones and virus infection in transgenic *N. benthamiana* leaves at 3 dpi. Effect of each hormone on GUS activity was assayed at least three times in four independent experiments. The GUS activity, 4-MU nmol-produced min⁻¹ mg⁻¹ protein, is represented as the mean \pm SD. Data are mean \pm SD, * $p < 0.05$, ** $p < 0.01$, *** $p < 0.001$ by Student *t*-test, respectively. ns = non-significant. (D) The content of endogenous SA and (E) JA levels in *N. benthamiana* during the infiltration of EV (pKn) and CymMV infection at 12, 24, and 72 hr. The intensity of SA and JA was measured by the ultra-high performance liquid chromatography-electrospray ionization tandem mass spectrometry (UHPLC-ESI-MS/MS) method.

Consequently, we examined the expression profile of *N. benthamiana* nonexpressor of pathogenesis-related genes-1 (*NbNPR1*) (SA marker gene), allene oxide synthase 2 (*NbAOS2*), lipoxygenase 2 (*NbLOX2*) (JA biosynthesis genes), 9-cis-epoxycarotenoid dioxygenase *NbNCED3*, and zeaxanthin epoxidase (*NbZEP*) (ABA biosynthesis genes) during exogenous application of SA (1 mM), MeJA (100 μ M), and ABA (100 μ M) at 24 hpi. Real-time qRT-PCR results showed that *NbNPR1*, *NbAOS2*, and *NbLOX2* were significantly upregu-

lated, whereas *NbNCED3* and *NbZEP* were not upregulated (Supplementary Figure S11). This indicates that the exogenous application of SA and MeJA significantly upregulated and induced *pPaAGO5b_941*, which may be due to SA- and MeJA-responsive elements (Supplementary Figure S12).

To measure endogenous SA and JA levels, *N. benthamiana* leaves were vacuum-infiltrated with EV (pKn) and CymMV infectious clones. After infiltration, leaf samples were collected at 12, 24, and 72 h, and SA and JA contents were measured using UHPLC-ESI-MS/MS. The intensity of SA was not detected in EV vector-treated leaves at 12 and 24 h, but it significantly increased at 72 h compared with CymMV-treated leaves. However, at 24 h, the intensity of SA was significantly higher in the CymMV-treated leaves than in the EV leaves (Figure 7D). In addition, the JA intensity was significantly enhanced at 12 and 72 h in CymMV-treated leaves compared with EV-treated leaves. However, at 24 h, JA intensity was significantly decreased in CymMV-treated leaves compared to EV-treated leaves (Figure 7E). We hypothesized that SA and JA act antagonistically during CymMV infection based on this endogenous measurement of SA and JA. Further experiments are needed to analyze the underlying molecular mechanism of action between SA and JA during CymMV infection.

2.9. Effect of *PaMYB30* on *PaAGO5b* Expression and Accumulation of CymMV in *P. aphrodite* subsp. *formosana*

In silico analysis of protein similarity of NbMYB30 in Orchidstra 2.0 [34] revealed that *P. aphrodite* subsp. *formosana* MYB30 (*PaMYB30*) (PATC157886) shares 52% protein similarity with NbMYB30, making *PaMYB30* the closest relative of NbMYB30 in orchids. Therefore, we speculated that *PaMYB30* is a candidate that responds to CymMV infection and activates the expression of endogenous *PaAGO5b*, as observed in *N. benthamiana* leaves. To verify this hypothesis, we inoculated *P. aphrodite* subsp. *formosana* leaves with a CymMV infectious clone via agro-infiltration and collected leaves to analyze expression profiles of *PaMYB30* and *PaAGO5b* at 12, 24, 48, and 72 h post-inoculation (hpi). Real-time qRT-PCR analysis indicated that the accumulation of *PaAGO5b* transcript was significantly elevated at 48 and 72 hpi (Figure 8A), as observed previously [33]. However, the accumulation of *PaMYB30* transcript increased in inoculated leaves at 24 and 48 hpi but decreased at 12 and 72 hpi (Figure 8B). The fluctuation of *PaMYB30* occurred at least 24 h earlier than that of *PaAGO5b* after CymMV inoculation, suggesting that *PaMYB30* could respond to virus infection.

Next, we investigated the causation between *PaMYB30* and *PaAGO5b* expression. We overexpressed FLAG-tagged *PaMYB30* and a PVY silencing suppressor, HC-pro, used to improve protein expression in CymMV-inoculated *P. aphrodite* subsp. *formosana* leaves. We found that the overexpression of *PaMYB30* did not alter the expression level of *PaAGO5b* (Figure 8C) but unexpectedly resulted in a reduction in CymMV accumulation (Figure 8E). Before analyzing CymMV accumulation during *PaMYB30* overexpression, we confirmed CymMV expression in *P. aphrodite* subsp. *formosana* leaves (Figure 8D). To verify these results, *PaMYB30* was silenced using the VIGS vector pKFV [35]. Real-time qRT-PCR analysis showed that *PaMYB30* expression was efficiently silenced by VIGS (Figure 8F); however, *PaAGO5b* expression was significantly upregulated (Figure 8F). To clarify the role of *PaMYB30* in plant defense systems, *PaMYB30*-silenced and mock-inoculated leaves (agroinfiltrated with empty VIGS vector, pKFV) were inoculated with CymMV. After quantifying viral accumulation, we found that *PaMYB30* knockdown contributed to a higher accumulation of CymMV (Figure 8G).

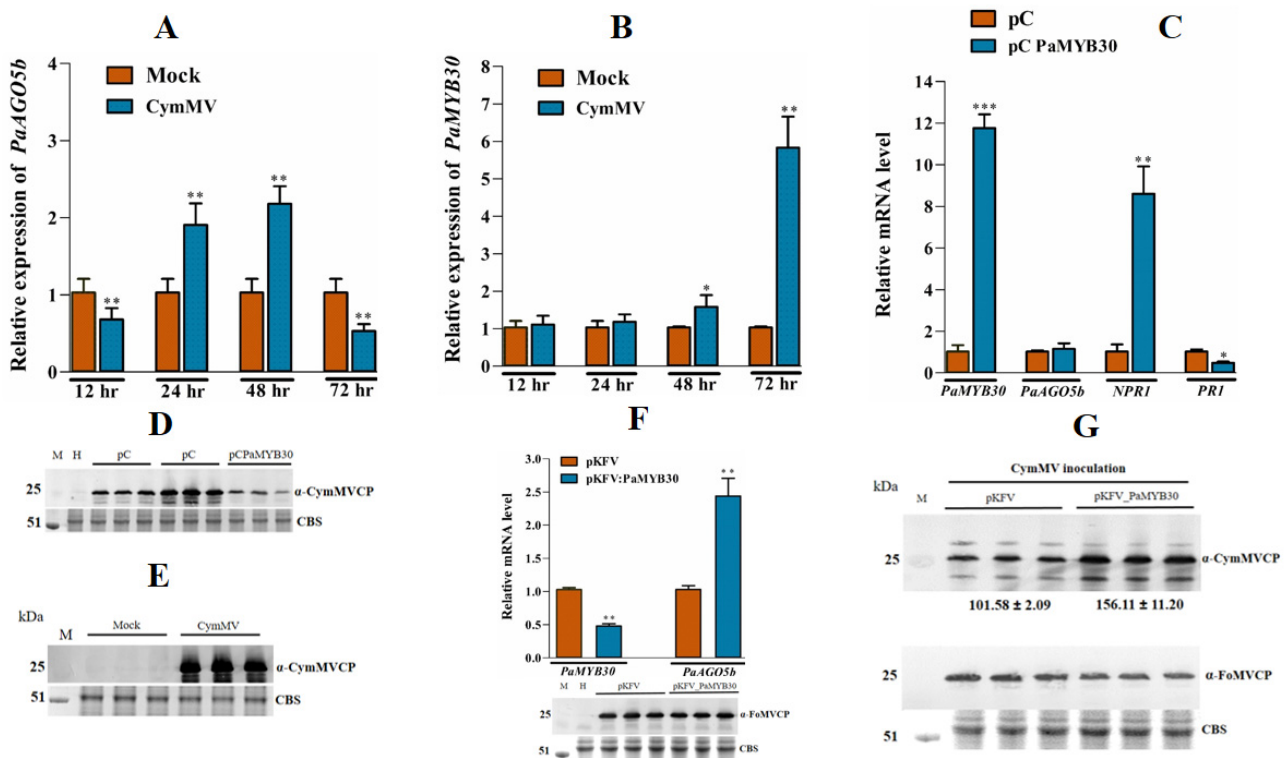


Figure 8. Expression profile of *PaAGO5b*, *PaMYB30*, and CymMV accumulation in CymMV infected leaves. (A) Expression profile of *PaAGO5b* and (B) *PaMYB30* in the *P. aphrodite* subsp. *formosana* leaves infiltrated with mock (pKn) or CymMV infectious clone. (C) The transcript accumulation of *PaAGO5b*, *PaNPR1*, and *PaPRI* during *PaMYB30* overexpression. For the *PaMYB30* overexpression analysis, *P. aphrodite* subsp. *formosana* leaves were infiltrated with empty vector pCambia-UbI1-ZsGFP vector (pC) or *PaMYB30* expression vector pC *PaMYB30*. (D) The accumulation of CymMV in CymMV infected leaves at 72 hpi was analyzed by Western blot. (E) The accumulation of CymMV during *PaMYB30* overexpression leaves at 72 hpi was analyzed by Western blot. (F) *PaMYB30* and *PaAGO5b* transcript accumulation during *PaMYB30* silencing at 10 dpi was analyzed using real-time qRT-PCR. (G) The CymMV accumulation in the *PaMYB30*-silenced leaves. The *PaMYB30* silenced leaves were further agroinfiltrated with CymMV infectious clone at 10 dpi (days post infiltration of agrobacterium EHA105 harboring pKFV or pKFV-MYB30 vector). The leaves were collected at 15 dpi, and the CymMV accumulation in the leaves was analyzed using Western blot. The FoMV accumulation in the leaves was analyzed using Western blot. For real-time qRT-PCR, the expression levels of each transcript, presented as normalized fold changes relative to that from mock-inoculated leaves (Mock) or EV are shown. Values are means \pm SD of three biological replicates. Data are mean \pm SD, * $p < 0.05$, ** $p < 0.01$, *** $p < 0.001$ by Student *t*-test, respectively. For Western blot, the accumulation of FoMV and CymMV were detected by respective specific anti-serum, α -FoMV CP and α -CymMV CP. Rubisco was stained with Coomassie-brilliant-blue and shown as a loading control.

2.10. Effects of *NbMYB30*, *NbNAC42*, and *NbZFP3* Expression on the Accumulation of CymMV in *P. aphrodite* subsp. *formosana*

To verify the function of *NbMYB30* in CymMV accumulation in *P. aphrodite* subsp. *formosana*, we overexpressed FLAG-tagged *NbMYB30* in *P. aphrodite* subsp. *formosana* and evaluated its effect on CymMV accumulation. Moreover, our previous experiments demonstrated that the TFs *NbNAC42* and *NbZFP3* might participate in the activation of *NbAGO5* expression during BaMV infection (provisionally accepted). Thus, these two TFs were also expressed in *P. aphrodite* subsp. *formosana* and subjected to the same evaluation as *NbMYB30*. For CymMV accumulation, a slight reduction was shown in *NbMYB30* expressing leaves (Supplementary Figure S13); however, 2.4- and 2.6-fold increases were observed in *NbNAC42*- and *NbZFP3*-expressing leaves (Supplementary Figure

S13). These results demonstrated that NbMYB30 physically interacts with the PaAGO5b promoter and participates in specific resistance mechanisms in *P. aphrodite* subsp. *formosana*. However, the NbNAC42 and NbZFP3 transcription factors may not function properly in exogenous environments.

3. Discussion

Transcription regulation is a crucial process that is affected by gene promoters. Appropriate studies on promoter activity during viral infection have not been found for plants, except for a few studies [21,36]. Recently, we identified the induced activity of NbAGO5 through the binding of TF NbNAC42 and repressed the activity by the binding of TF NbZFP3 (provisionally accepted). Promoter sequence analysis of NbAGO5 and *pPaAGO5b* shows that the sequence identity between these two promoters is around 30% only. Moreover, presence of *cis*-acting element in the promoter region is also diverse. Experimental findings from *Arabidopsis*, rice, *N. benthamiana*, and orchids showed that AGOs play a key role in antiviral defense mechanisms. The results of this study revealed the effect of viruses on AGO promoter activity through the analysis of *pPaAGO5b*.

CymMV and ORSV contain monopartite, positive-sense RNA genomes, and are the most widespread and economically significant viruses among 50 orchid-infecting viruses [32]. In addition to their natural hosts, CymMV and ORSV can infect *N. benthamiana*, frequently used as a systemic host in plant virus research [37]. Owing to the slow growth of *P. aphrodite* subsp. *formosana*, we performed experiments on *N. benthamiana* to test the activity of the *pPaAGO5s* constructs fused with GUS. To interpret the differential expression patterns of GUS driven by *pPaAGO5a*, *pPaAGO5b*, and *pPaAGO5c*, we compared the promoter sequences (Supplementary Tables S1–S3). Preliminary GUS activity analysis showed that *pPaAGO5b* was significantly enhanced during CymMV and ORSV infection compared to *pPaAGO5a* and *pPaAGO5c* (Figure 1A,B). These results are consistent with those of previous studies [33]. The supported results from PaAGO5b expression [37] and current *pPaAGO5b* fluorescent quantitative analyses suggest that PaAGO5b may serve as the first layer of the immune system during viral infection. The highest activity of *pPaAGO5b* may be due to the presence of some critical variances in the spreading of putative *cis*-acting elements, such as ABRE, TGACG motif, and TGA- and TCA-elements, which are absent in *pPaAGO5c*, or GARE-motif and TCA-elements, which are absent in *pPaAGO5a* (Supplementary Tables S1–S3). The tissue-specific expression profile revealed that the higher expression of GUS driven by *pPaAGO5b* (Figure 2) indicates that PaAGO5b may play a key role during plant growth and development. However, the roles of *pPaAGO5a* and *pPaAGO5c* in plant growth and development need to be explored.

Early enhanced activity of *pPaAGO5b* was observed during CymMV, ORSV, BaMV, TMV, and FoMV, but not PVX infection in *N. benthamiana* (Figure 3A). In contrast, *Arabidopsis* AGO5 expression was induced by PVX infection. In particular, AtAGO2 and AtAGO5 are required to fully restrict PVX infection in systemic tissues [7]. This finding may be due to the different host–factor interactions during PVX infection. *pPaAGO5b* activity was significantly increased by the overexpression of CymMV_CP, CymMV_TGBp1, ORSV_CP, and ORSV_MP (Figure 3B). Principally, GUS activity was significantly enhanced during CymMV infection, and the expression of CymMV_TGBp1 and ORSV_MP (Figure 3A,B). This finding may be due to CymMV accumulation at the initial to middle stages of infection, which increases the activity of *pPaAGO5b*. Previous studies have shown that PaAGO5b expression is significantly elevated when *P. aphrodite* subsp. *formosana* plants are singly infected with CymMV [33]. The higher activities of CymMV_TGBp1 and ORSV_MP on *pPaAGO5b* indicate that these two viral proteins are crucial for inducing *pPaAGO5b*. However, there was no direct proof that CymMV_TGBp1 or ORSV_MP was involved in suppressing RNA silencing. This indicates that PaAGO5b may act as a lead protein in controlling viral infections. We demonstrated a significant increment in the expression of NbAGO5 during BaMV_TGBp1 overexpression (provisionally accepted). BaMV and

CymMV belong to the genus *potexvirus*, and TGBp1 may act as a major inducer of AGOs during potexvirus infection.

From the early induced activity of *pPaAGO5b*, we further mapped the virus-responsive element of *pPaAGO5b* toward viral infection. Transient expression analysis revealed that the 5'-deletion construct, *pPaAGO5b_941*, showed significantly higher activity toward CymMV (Figure 4A), ORSV infection (Figure 4D), and the expression of viral genes such as CymMV_CP (Figure 4B), CymMV_TGBp1 (Figure 4C), ORSV_CP (Figure 4E), and ORSV_MP (Figure 4F). The higher activity of *pPaAGO5b_941* may be due to the core-and stress-related *cis*-acting elements within this region (Supplementary Table S2).

Previous studies of virus infection on plant AGO genes did not distinguish a direct or indirect virus-induced effect. To explore this, we cloned the viral genes for Y1H analysis. Based on Y1H analysis, we found that viral proteins did not directly interact with *pPaAGO5b_941* (Figure 5A). Furthermore, screened TFs expression profiles were analyzed, and the results showed that NbREV8 and NbMYB30 were significantly enhanced during CymMV infection (Supplementary Figure S8); however, Y1H analysis showed that only NbMYB30 physically interacted with *pPaAGO5b_941* (Figure 5A). NbREV8 may interact with other AGOs or pathogen-related genes during viral infections. However, there are no prior studies on the role of the NbMYB30 TF in AGO gene expression during viral infection. Real-time qRT-PCR and Y1H analysis revealed that NbMYB30 might be upregulated during viral infection and directly binds to the region of *pPaAGO5b_941* to regulate PaAGO5b expression. The putative MYB-binding site AACAAA reported to be targeted by MYB30 [38] was found at position 584 in *pPaAGO5b_941*. It is possible that the NbMYB30 TF binds to the AACAAA site to induce PaAGO5b at the time of infection. Furthermore, NbMYB30 overexpression (Figure 6A) and VIGS analysis (Figure 6C) in *N. benthamiana* revealed that NbMYB30 positively regulated *pPaAGO5b* in response to viral infections.

NbMYB30 belongs to the R2R3 MYB TF and is part of the MYB TF family. The MYB TF family plays a significant role in plant immune responses to biotic and abiotic stresses [39–42]. Published research findings on MYB TFs involved in the defense response to viral invasion are currently limited. However, inducible NtMYB1 has been identified in tobacco during TMV infection [25]. Tomato MYB28 TF (SIMYB28), and an R2R3-MYB TF expression level was strongly induced by *Tomato yellow leaf curl virus* (TYLCV) infection in tomato [26]. In addition, upregulation of AtMYB96 has been reported to be induced upon *Cauliflower mosaic virus* gene VI (P6) infection [43] in *Arabidopsis*. A total of 18 differentially expressed MYB TFs have been identified in watermelon during the invasion of *Cucumber green mottle mosaic virus* (CGMMV) [24]. Among them, 15 and 3 MYB TFs were up- and downregulated, respectively, in the leaf tissues of watermelon. These published results and current findings emphasize the role of MYB TF family proteins during virus infection.

The plant hormones SA, JA, and ABA, play key roles in helping plants balance their responses to viral stress [16–18,44]. Owing to hormone-responsive elements, *pPaAGO5b_941* (Supplementary Figure S12) may affect various phytohormone-related metabolic activities during viral stress. We evaluated the effect of exogenous application of SA (1 mM), MeJA (100 μ M), and ABA (100 μ M) in *N. benthamiana*. GUS activity driven by *pPaAGO5b_941* was significantly upregulated after exogenous application of SA (Figure 7A) and MeJA (Figure 7B) but not ABA (Figure 7C). The expression profile of *NbNPR1*, *NbAOS2*, *NbLOX2*, *NbNCED3*, and *NbZEP* showed that *NbNPR1*, *NbAOS2*, and *NbLOX2* were significantly upregulated, whereas *NbNCED3* and *NbZEP* were not enhanced (Supplementary Figure S11). This indicates that the exogenous application of SA and MeJA significantly upregulated and induced *pPaAGO5b_941*, which may be due to SA- and MeJA-responsive elements (Supplementary Figure S12). Furthermore, we assumed that SA and JA have a possible role in defense mechanisms during viral infection. We noticed that the combination of MeJA and CymMV or ORSV increased the activity of GUS when compared with the exogenous application of MeJA or virus infection alone (Figure 7B). Similar GUS activities were not observed with the application of SA or ABA in combination with CymMV and ORSV (Figure 7A,C). The significant increase in the activity of *pPaAGO5b_941* after MeJA

application during viral infection indicates that MeJA acts as a major hormone in viral defense mechanisms. However, SA application alone increased the *pPaAGO5b_941* activity level (Figure 7A) compared to the combination of virus infection, which needs to be further explored.

To validate the antagonistic relationship, endogenous SA and JA levels were measured. In *N. benthamiana*, the CymMV-inoculated experiments revealed that the accumulation of SA and JA was typically antagonized (Figure 7D,E), as reported in previous studies [45]. The SA level at 12 hpi in the EV- or CymMV-inoculated leaves was lower than the detection limit of our mass spectrometer (Figure 7D). The SA level at 24 hpi in EV-inoculated leaves remained undetectable but could be detected in CymMV-inoculated leaves at 24 hpi (Figure 7D). However, when comparing the JA level in CymMV-inoculated leaves to that in EV-inoculated leaves, it was higher at 12 hpi but lower at 24 hpi (Figure 7E). However, the SA and MeJA signaling pathways sometimes affect each other through a complex network of synergistic and antagonistic interactions [46,47]. Even though the TCA-element and TGACG motifs are present at the core promoter region of *pPaAGO5b_941* (Supplementary Figure S12), the enhanced GUS activity under MeJA indicates its significance during virus infection. A few studies have revealed that regulatory networks enhance RNA-silencing activity via JA signaling. For instance, in rice, OsAGO18 promotes antiviral defense against RSV via transcriptional activation by jasmonate signaling [21]. The exogenous supply of MeJA efficiently reduces RBSDV infection in rice, whereas inhibition of the JA response enhances RBSDV infection [48,49]. Further investigation is required to investigate the crosstalk between SA and JA and the underlying molecular mechanism of these hormones on PaAGO5b activity during viral infection. Although we did not perform hormone analyses on *P. aphrodite* subsp. *formosana*, it was evident that PaMYB30 was suppressed at 12 hpi and activated at 24 hpi (Figure 8B).

This study revealed that the expression profiles of PaMYB30 and PaAGO5b are negatively correlated during CymMV infection. Considering that a distinct physical interaction between NbMYB30 and *pPaAGO5b_941* was demonstrated (Figure 5A), the exogenous expression of NbMYB30 served as an activator of *pPaAGO5b_941*. Therefore, we cannot exclude the possibility that PaAGO5b expression is controlled by a potential suppressor element that lies outside the *pPaAGO5b_941* region or the interaction of PaMYB30 with the potentially endogenous regulator in *P. aphrodite* subsp. *formosana*. Thus, PaAGO5b expression could only be activated when PaMYB30 levels decreased (Figure 8F). However, CymMV accumulation was significantly lower with PaMYB30 overexpression (Figure 8E) and higher with PaMYB30 silencing (Figure 8G). Although PaMYB30 has a significant defense role during viral infection in *P. aphrodite* subsp. *formosana*, with PaMYB30 expression, the nature of the antiviral response in orchid under PaMYB30 regulation remains unclear. The *P. aphrodite* subsp. *formosana* NPR1 and PR1 expression levels were significantly up- and downregulated, respectively, with the overexpression of PaMYB30 (Figure 8C), indicating PaMYB30 may cast regulatory antiviral activity through NPR1/PR1-related pathway. NbMYB30 overexpression in *P. aphrodite* subsp. *formosana* resulted in a slight decrease in CymMV accumulation (Supplementary Figure S13) compared with NbNAC42 and NbZFP3, a proven activator and repressor of NbAGO5 (provisionally accepted), indicating that NbMYB30 acts as an activator of PaAGO5b during viral infection. Our findings provide further insight into the role of PaMYB30 during virus infection and the defense response upon orchid–virus interactions.

In the current study, we characterized and functionally validated *pPaAGO5b* in *N. benthamiana* during viral infection (Figure 9).

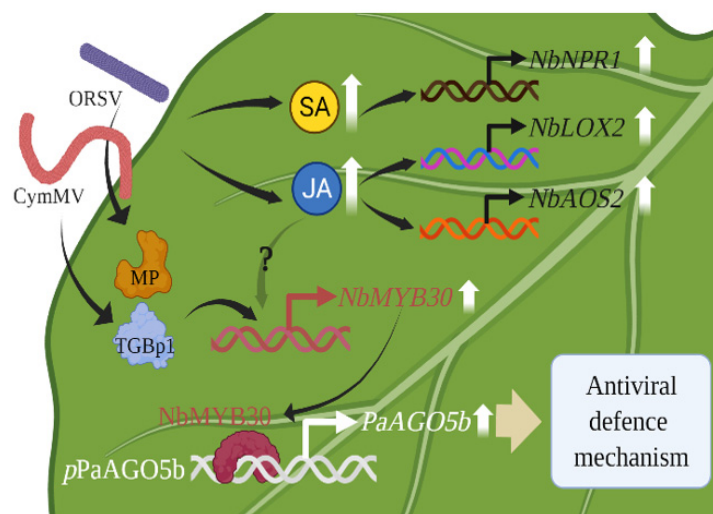


Figure 9. A model for enhancing antiviral defense mechanism through the activation of *pPaAGO5b*. The CymMV or ORSV infectious clones and their TGBp1, a CymMV-encoded protein, and MP, an ORSV-encoded protein, may upregulate plant defense-related TF NbMYB30. The NbMYB30 TF binds to the *pPaAGO5b* (*p*-indicates the promoter) and transcriptionally activates PaAGO5b expression to enhance the antiviral defense mechanism. During virus infection, phytohormones SA and JA and their marker genes were upregulated. Principally, JA was significantly enhanced; however, upregulation of NbMYB30 under JA enhancement during virus infection has not yet been explored. LOX2—lipoxygenase 2; AOS2—allene oxide synthase 2, NPR1—nonexpressor of pathogenesis-related genes-1.

GUS fluorescence analysis of stably transformed *N. benthamiana* leaves revealed that *pPaAGO5b* was induced during CymMV and ORSV infection and overexpression of viral genes; notably, during CymMV, CymMV_TGBp1, and ORSV_MP. The 5'-deletion fragment analysis showed that *pPaAGO5b_941* had a higher inducible activity. Y1H analysis showed that viral infection indirectly induced the activity of *pPaAGO5b_941* through the interaction of NbMYB30 TF, an activator of *pPaAGO5b_941*. An exogenous supply of SA, MeJA, and ABA in transgenic *N. benthamiana* showed that SA and MeJA induced *pPaAGO5b_941*. However, the combination of phytohormones and CymMV and ORSV infection revealed that MeJA was significantly enhanced, indicating that JA is the primary hormone inducing *pPaAGO5b_941* during viral infection. This can help understand the molecular mechanism of PaAGO5b in RNA silencing during virus invasion. Furthermore, the thorough understanding of the regulatory mechanism may benefit the development and application of *pPaAGO5b* as an inducible promoter in the future.

4. Materials and Methods

4.1. Cloning and In Silico Exploration of the PaAGO5s Promoter

Genomic DNA from *P. aphrodite* subsp. *formosana* leaves was extracted using the CTAB method [50], and used as a template for cloning promoter sequences. The primers (Supplementary Table S4) used for amplifying the putative promoter sequences of PaAGO5a, PaAGO5b, and PaAGO5c were designed from the translational start site, ATG, to about 2000 nucleotides upstream of each gene. After PCR amplification, the positive DNA fragments of PaAGO5a, PaAGO5b, and PaAGO5c were purified and separately ligated into a T&A cloning vector (YEASTERN Biotech Co., Ltd., Taipei City, Taiwan). The cloned fragments were sequenced and confirmed using the BLAST search against the Orchidstra 2.0 database [34]. Furthermore, the transcription start sites (TSS) of the PaAGO5a, PaAGO5b, and PaAGO5c promoters were confirmed by 5'-rapid amplification of cDNA ends (5'-RACE, Takara Bio, San Jose, CA, USA).

To predict the *cis*-acting regulatory elements present in the cloned PaAGO5s promoter region, we used *in silico* analysis in PlantCARE (<http://bioinformatics.psb.ugent.be/webtools/plantcare/html/> accessed on 20 June 2022) [51].

4.2. Construction of pPaAO5s::GUS Fusion Vectors

A 2759-bp *HindIII*-*NcoI* fragment containing pPaAGO5a, a 2029-bp *XbaI*-*NcoI* fragment containing pPaAGO5b, and a 2589-bp *PstI*-*NcoI* fragment containing pPaAGO5c were sliced from the T&A cloning vector and subcloned into the same sites as the binary vector pCambia1305.2 (Marker Gene Technologies, Eugene, OR, USA) after enzymatic digestion to replace the CaMV 35S promoter, which controls the expression of the GUS plus gene. The resulting constructs were named pCambia-pPaAGO5a::GUS, pCambia-pPaAGO5b::GUS, and pCambia-pPaAGO5c::GUS, respectively. The vector pCambia1305.2 with the CaMV 35S promoter was used as a positive control (CaMV 35S). The promoter-less vector pCambia1391Z was used as the negative control.

4.3. In Planta Agrobacterium-Mediated Transformation of *N. benthamiana* Plants

The constructed pCambia-pPaAGO5a::GUS, pCambia-pPaAGO5b::GUS, and pCambia-pPaAGO5c::GUS plasmids were introduced into the *Agrobacterium tumefaciens* culture GV3850 individually by electroporation [52]. *A. tumefaciens*-mediated transformation procedures were performed as previously described [53]. Transformants were regenerated using the method described [54]. T₀ positive transformants were screened for *hygromycin* (*HygR*) resistance [55]. The T₁ and T₂ positive transformants were confirmed by PCR amplification (primers used are listed in Supplementary Table S5) and GUS staining and grown to generate T₃ transgenic plants. Homozygous transgenic lines of the T₃ generation were chosen for subsequent investigation via segregation ratio analysis.

4.4. Construction of pPaAGO5b Deletion Promoters::GUS Fusion Vectors

Ten 5'-truncated pPaAGO5b fragments of different sizes (−1782, −1582, −1182, −941, −582, −349, −235, −109, −88, and −65 bp to −1 bp) were amplified from the pPaAGO5b full-length promoter and subcloned into the *XbaI*-*NcoI* sites of pCambia1305.2 by replacing the original CaMV 35S promoter (primers used are listed in Supplementary Table S6).

4.5. Construction of Virus Gene Plasmids and Agroinfiltration of Virus Infectious Clones and Viral Genes into Transgenic *N. benthamiana*

Different infectious clones, including CymMV [35], ORSV [35], BaMV [56], PVX [57], TMV, and *Foxtail millet mosaic virus* (FoMV) [35] used in this study were mainly based on the backbone vector pKn [58]. Therefore, for the overexpression of viral genes such as CymMV coat protein (CymMV_CP; 672 bp), CymMV triple gene block protein 1 (CymMV_TGBp1; 702 bp), ORSV coat protein (ORSV_CP; 477 bp), and ORSV movement protein (ORSV_MP; 840 bp), the corresponding coding regions were amplified from the CymMV and ORSV full-length infectious clones and cloned into the plasmid pEPYON-32K [59] with the CaMV 35S promoter. The primers used for cloning viral genes are listed in Supplementary Table S7.

To analyze the stress responses caused by viruses and viral genes, *A. tumefaciens* strain GV3850 cells harboring infectious clones of CymMV, ORSV, BaMV, PVX, TMV, FoMV, and viral gene expression constructs were agroinfiltrated into *N. benthamiana* plants [15]. The *A. tumefaciens* cultures were collected by centrifugation, resuspended in infiltration buffer (10 mM MES buffer, pH 5.5, and 10 mM MgCl₂), adjusted to OD₆₀₀ = 0.5, and agroinfiltrated into the leaves of each test plant using a needleless syringe. The leaves were harvested three days post-inoculation (dpi) and subjected to the GUS activity assay.

4.6. GUS Histochemical Staining and Fluorescent Quantitative Assay

The GUS staining and activity of infiltrated constructs were estimated by the standard method [60]. The fluorescence was measured at excitation and emission wavelengths of

365 nm and 455 nm using a fluorimeter (SpectraMax M2, San Jose, CA, USA). GUS activity was calculated as nmol 4-methylumbelliferone (4-MU)-generated $\text{min}^{-1} \text{mg}^{-1}$ protein.

4.7. Identification of Transcription Factors (TFs) and Yeast One-Hybrid (Y1H) Analysis

PlantPan 3.0 (<http://plantpan.itps.ncku.edu.tw/> accessed on 20 June 2022) [61] was used to identify co-expressed TFs with the PaAGO5b promoter. By selecting hormone treatment conditions, we obtained a list of TFs from *Arabidopsis* that were co-expressed with the queried promoter sequence, as indicated by a Pearson correlation coefficient with a *p*-value > 0.9. To obtain a short list of TFs regulated only by ABA, MeJA, and SA, gene ontology and functional descriptions of these TFs were queried manually. Finally, a total of five TFs (MYB94, REV8, late elongated hypocotyl, and circadian clock associated-1-like protein 1, MYB30, and Circadian 1 (CIR1) transcription factor) were selected from *Arabidopsis*, and their full-length nucleotide sequences were used as a template to retrieve the TFs sequences (Supplementary Table S8) from *N. benthamiana* using draft genome sequence database (https://solgenomics.net/organism/Nicotiana_benthamiana/genome accessed on 20 June 2022).

To determine the interaction between pPaAGO5b and viral genes or TFs, we performed Y1H assay. The pPaAGO5b_941 sequence was cloned into the yeast reporter vector pHIS2.1-BD (Clontech Laboratories, Inc., San Jose, CA, USA) after digestion with the *SacI* and *EcoRI* enzymes. Full-length coding regions of the viral genes and TFs were amplified and cloned into the pGADT7-AD vector (Clontech Laboratories, Inc., CA, USA). After confirming the sequence orientation of the cloned viral genes and TFs, the pHIS2.1 vector containing the pPaAGO5b_941 was cotransformed individually with the pGADT7-viral genes and TFs into *Saccharomyces cerevisiae* strain Y187. Serial dilution transformant growth assays evaluated Protein-DNA interactions on SD/–Leu/–Trp/–His plates supplemented with 20 mM 3-AT. The primers used for the TFs amplification are listed in Supplementary Table S9.

4.8. Transient Expression and Virus-Induced Gene Silencing (VIGS) of NbMYB30

To overexpress FLAG-NbMYB30 in *N. benthamiana*, plasmid pEPFlag-NbMYB30 was generated. The coding sequence (CDS) for NbMYB30 (1083 bp) was amplified from *N. benthamiana* cDNA using PCR (primers used are listed in Supplementary Table S10). The PCR product was gel-purified, digested with *PstI* and *SacI*, and used to replace the corresponding fragments in pEP-mGFP [59]. For overexpression, pEPFlag-NbMYB30 was introduced into *A. tumefaciens* strain GV3850 by electroporation. *A. tumefaciens* cultures were collected by centrifugation and resuspended in an infiltration buffer. Suspensions were adjusted to $\text{OD}_{600} = 0.5$ and infiltrated by a needleless syringe into the leaves of each test plant.

Tobacco rattle virus (TRV)-based VIGS was used to knockdown the expression of NbMYB30. A 240-bp fragment of the NbMYB30 3' untranslated region (UTR) sequence was amplified by PCR using *N. benthamiana* cDNA as a template (primers used are listed in Supplementary Table S10). The amplified PCR product was gel-purified, digested with *EcoRI* and *BamHI*, and cloned into the pTRV2 plasmid [62] to generate pTRV2-NbMYB30. The pTRV1- and pTRV2-based constructs were electroporated into the *A. tumefaciens* strain C58C1 for knockdown experiments, as previously described [57].

4.9. Agroinfiltration and Virus Inoculation in *P. aphrodite* subsp. *formosana*

Agroinfiltration of *P. aphrodite* subsp. *formosana* leaves were performed as reported by [33]. Briefly, pCAMBIA-Ubi1-ZsGFP, pCAMBIA-Ubi1-PaMYB30, and CymMV infectious constructs were electroporated into *A. tumefaciens* strain EHA105. Aliquots of a 2 mL saturated culture of agrobacteria were poured into an 18 mL LB medium containing ampicillin and kanamycin and incubated at 28 °C for 3 h. Bacteria were then pelleted by centrifugation and incubated in AB-MES buffer with constant shaking (60 rpm) at 28 °C for 24 h. Finally, the bacteria were pelleted by centrifugation and resuspended in AB-MES+1/2 MS infiltration buffer containing 200 μM acetosyringone. The expression construct inocu-

lum was adjusted to give an OD₆₀₀ of 10. The inoculum containing the CymMV infectious clone was adjusted to an OD₆₀₀ value of 0.5. The coding sequence (CDS) for *PaMYB30* (912 bp) was amplified from *P. aphrodite* subsp. *formosana* cDNA using PCR (primers used are listed in Supplementary Table S11).

4.10. *PaMYB30* Gene VIGS Construct, pKFV-*PaMYB30*

The VIGS construct for the knockdown of *PaMYB30* in *P. aphrodite* subsp. *formosana* was constructed as previously reported [33]. Briefly, the 241 bp fragment covering the CDS and 3' UTR regions used for silencing *PaMYB30* was flanked by the *HpaI* restriction enzyme cut site through PCR amplification. After *HpaI* digestion, the fragment was ligated with *HpaI* digested pKFV [35] to generate pKFV-*PaMYB30*. The primers used for the pKFV-*PaMYB30* VIGS construct are listed in Supplementary Table S11.

4.11. RNA Isolation and Real-Time qRT-PCR

Total RNA was extracted from leaf tissues using the TriPure Isolation Reagent (Roche Life Science, St. Louis, MO, USA). Total RNA (2 µg) was reverse transcribed to cDNA using Superscript II RT (Invitrogen, Waltham, MA, USA). Real-time qRT-PCR analysis was performed using one-step real-time qRT PCR (Applied Biosystems, Waltham, MA, USA) with SYBR Green, as described previously [15]. Primers for TFs, GUS, and marker genes are listed in Supplementary Table S12. The expression levels of target transcripts were normalized to the geometric mean of the housekeeping gene, *Actin*, to control the variability and further analyzed using the $2^{-\Delta\Delta CT}$ method [63]. To confirm reproducibility, three biological replicates of each assay were used for real-time qRT-PCR analysis, and three technical replicates were analyzed for each biological replicate.

4.12. Hormonal Treatment

For hormonal treatment, 28-day-old transgenic *N. benthamiana* plants were sprayed individually with SA (1 mM), MeJA (100 µM), and ABA (100 µM) and infiltrated with CymMV and ORSV infectious clones independently. Another set of plants was infiltrated and sprayed with a combination of viruses and hormones.

4.13. Phytohormone Extraction

For phytohormone extraction from *N. benthamiana* leaves, a previously published method [64] with slight modifications was employed. Briefly, 1 g of leaves was ground into powder in liquid nitrogen. The powder was soaked in a 5 mL extraction solvent (a mixture containing 2-propanol, H₂O, and 12 N HCl in a ratio of 2:1:0.002 by volume) and vigorously shaken for 30 min at 4 °C. Leaf tissues were then pelleted by centrifugation at 10,000 × g, 4 °C for 10 min and further filtered using Miracloth (125 µm pore size). The resulting solution was passed through a C18 column (Avantor™ BAKERBOND™ spe Octadecyl (C18) Disposable Extraction Columns, Thermo Fisher Scientific Inc, Waltham, MA, USA) to remove the chlorophyll. Then 10 mL dichloromethane was added to the filtrate and vigorously shaken for 30 min at 4 °C, followed by centrifugation at 10,000 × g, 4 °C for 10 min. Two phases were subsequently formed, and the lower phase containing the phytohormones mixture was collected. The solvent of the mixture was evaporated using nitrogen blow-down. The sample was re-dissolved in 100 µL methanol and stored at −80 °C until UHPLC-ESI-MS/MS analysis.

4.14. UHPLC-ESI-MS/MS Analysis of Salicylic Acid and Jasmonic Acid

Phytohormones were measured using a Thermo Scientific Dionex UltiMate 3000 system (Thermo Fisher Scientific Inc.) linked to an amaZon speed-ion trap mass spectrometer (Bruker, Billerica, MA, USA) equipped with electrospray ionization (ESI). Salicylic acid and jasmonic acid were separated using an ODS column (AQUITY UPLC BEH shield RP18, 1.7 µm, 2.1 × 100 mm, Waters, BA, UK) with a biphasic solvent system consisting of 0.1% (v/v) formic acid in ddH₂O (A) and 100% acetonitrile (B) at a 0.3 mL min^{−1} flow rate. The linear

gradient was set according to the following profile: 0 min, 100% A; 2 min, 60% A + 40% B; 5 min, 40% A + 60% B; 13 min, 100% B, and then kept for 2 min and equilibrated for 5 min before the next injection. The injection volume used was 20 μ L. The column oven temperature was set to 40 °C. The mass spectrometer parameters were as follows: 4.5 kV capillary; 500 V endplate offset voltage; 40.0 psi nebulizer pressure; 8.0 L min⁻¹ dry gas, 230 °C dry temperature. The full scan was set at 40–300 m/z. In negative mode, ESI-MS/MS was operated in multiple reaction monitoring (MRM). MRM was set at 137–93 m/z to detect salicylic acid and 209–165 m/z to detect jasmonic acid.

4.15. Statistical Analysis

All the GUS quantitative experiments were performed three times. Data are presented as the mean \pm SD. Treatment means were further compared by one-way analysis of variance with Student's *t* test using GraphPad Prism 8.1.2 (GraphPad Software, La Jolla, CA, USA); differences with *p* values < 0.05 were considered significant.

Supplementary Materials: The following supporting information can be downloaded at: <https://www.mdpi.com/article/10.3390/ijms23179825/s1>.

Author Contributions: K.K.V. and S.-Y.K. performed the experiments and wrote the article. N.-W.T. and S.-Y.W. performed and analyzed the hormonal data. Y.-W.H., C.-C.H., Y.-H.H. and N.-S.L. designed the research, took part in data analysis, and edited the manuscript. All authors have read and agreed to the published version of the manuscript.

Funding: This work was financially supported in part by the Ministry of Science and Technology, Taiwan (MOST-110-2313-B-005-019), the Advanced Plant Biotechnology Center from The Featured Areas Research Center Program within the framework of the Higher Education Sprout Project by the Ministry of Education (MOE) in Taiwan, and Innovative Translational Agricultural Research Program (2018PRE022, AS-108-ITAR-L022 and AS-109-ITAR-L022).

Institutional Review Board Statement: Not applicable.

Informed Consent Statement: Not applicable.

Data Availability Statement: Not applicable.

Acknowledgments: We thank Ming-Lun Chou, Department of Life Sciences, Tzu-Chi University, Taiwan for providing yeast vectors (pHIS2.1-BD and pGADT7-AD).

Conflicts of Interest: The authors declare that they have no conflict of interest.

References

1. McLeish, M.J.; Fraile, A.; García-Arenal, F. Evolution of plant–virus interactions: Host range and virus emergence. *Curr. Opin. Virol.* **2019**, *34*, 50–55. [[CrossRef](#)]
2. Baulcombe, D. RNA silencing in plants. *Nature* **2004**, *431*, 356–363. [[CrossRef](#)] [[PubMed](#)]
3. Li, F.; Wang, A. RNA-targeted antiviral immunity: More than just RNA silencing. *Trends Microbiol.* **2019**, *27*, 792–805. [[CrossRef](#)] [[PubMed](#)]
4. Ma, Z.; Zhang, X. Actions of plant Argonautes: Predictable or unpredictable? *Curr. Opin. Plant Biol.* **2018**, *45*, 59–67. [[CrossRef](#)] [[PubMed](#)]
5. Li, Z.; Li, W.; Guo, M.; Liu, S.; Liu, L.; Yu, Y.; Mo, B.; Chen, X.; Gao, L. Origin, evolution and diversification of plant ARGONAUTE proteins. *Plant J.* **2022**, *109*, 1086–1097. [[CrossRef](#)] [[PubMed](#)]
6. Qu, F.; Ye, X.; Morris, T.J. Arabidopsis DRB4, AGO1, AGO7, and RDR6 participate in a DCL4-initiated antiviral RNA silencing pathway negatively regulated by DCL1. *Proc. Natl. Acad. Sci. USA* **2008**, *105*, 14732–14737. [[CrossRef](#)] [[PubMed](#)]
7. Brosseau, C.; Moffett, P. Functional and genetic analysis identify a role for Arabidopsis ARGONAUTE5 in antiviral RNA silencing. *Plant Cell* **2015**, *27*, 1742–1754. [[CrossRef](#)]
8. Alazem, M.; He, M.-H.; Moffett, P.; Lin, N.-S. Abscisic acid induces resistance against bamboo mosaic virus through Argonaute 2 and 3. *Plant Physiol.* **2017**, *174*, 339–355. [[CrossRef](#)]
9. Wu, J.; Yang, Z.; Wang, Y.; Zheng, L.; Ye, R.; Ji, Y.; Zhao, S.; Ji, S.; Liu, R.; Xu, L. Viral-inducible Argonaute18 confers broad-spectrum virus resistance in rice by sequestering a host microRNA. *eLife* **2015**, *4*, e05733. [[CrossRef](#)]
10. Ghoshal, B.; Sanfaçon, H. Temperature-dependent symptom recovery in *Nicotiana benthamiana* plants infected with *Tomato ringspot virus* is associated with reduced translation of viral RNA2 and requires ARGONAUTE 1. *Virology* **2014**, *456*, 188–197. [[CrossRef](#)]

11. Scholthof, H.B.; Alvarado, V.Y.; Vega-Arreguin, J.C.; Ciomperlik, J.; Odokonyero, D.; Brosseau, C.; Jaubert, M.; Zamora, A.; Moffett, P. Identification of an ARGONAUTE for antiviral RNA silencing in *Nicotiana benthamiana*. *Plant Physiol.* **2011**, *156*, 1548–1555. [[CrossRef](#)] [[PubMed](#)]
12. Diao, P.; Zhang, Q.; Sun, H.; Ma, W.; Cao, A.; Yu, R.; Wang, J.; Niu, Y.; Wuriyangan, H. miR403a and SA are involved in NbAGO2 mediated antiviral defenses against TMV infection in *Nicotiana benthamiana*. *Genes* **2019**, *10*, 526. [[CrossRef](#)] [[PubMed](#)]
13. Bhattacharjee, S.; Zamora, A.; Azhar, M.T.; Sacco, M.A.; Lambert, L.H.; Moffett, P. Virus resistance induced by NB-LRR proteins involves Argonaute4-dependent translational control. *Plant J.* **2009**, *58*, 940–951. [[CrossRef](#)] [[PubMed](#)]
14. Takeda, A.; Iwasaki, S.; Watanabe, T.; Utsumi, M.; Watanabe, Y. The mechanism selecting the guide strand from small RNA duplexes is different among argonaute proteins. *Plant Cell Physiol.* **2008**, *49*, 493–500. [[CrossRef](#)]
15. Huang, Y.W.; Hu, C.C.; Tsai, C.H.; Lin, N.S.; Hsu, Y.H. *Nicotiana benthamiana* Argonaute10 plays a pro-viral role in *Bamboo mosaic virus* infection. *New Phytol.* **2019**, *224*, 804–817. [[CrossRef](#)]
16. Berens, M.L.; Berry, H.M.; Mine, A.; Argueso, C.T.; Tsuda, K. Evolution of hormone signaling networks in plant defense. *Annu. Rev. Phytopathol.* **2017**, *55*, 401–425. [[CrossRef](#)]
17. Alazem, M.; Lin, N.S. Roles of plant hormones in the regulation of host-virus interactions. *Mol. Plant Pathol.* **2015**, *16*, 529–540. [[CrossRef](#)]
18. Islam, W.; Naveed, H.; Zaynab, M.; Huang, Z.; Chen, H.Y. Plant defense against virus diseases; growth hormones in highlights. *Plant Signal. Behav.* **2019**, *14*, 1596719. [[CrossRef](#)]
19. Alazem, M.; Kim, K.H.; Lin, N.S. Effects of abscisic acid and salicylic acid on gene expression in the antiviral RNA silencing pathway in *Arabidopsis*. *Int. J. Mol. Sci.* **2019**, *20*, 2538. [[CrossRef](#)]
20. Li, W.; Cui, X.; Meng, Z.; Huang, X.; Xie, Q.; Wu, H.; Jin, H.; Zhang, D.; Liang, W. Transcriptional regulation of *Arabidopsis* miR168a and argonaute1 homeostasis in abscisic acid and abiotic stress responses. *Plant Physiol.* **2012**, *158*, 1279–1292. [[CrossRef](#)]
21. Yang, Z.; Huang, Y.; Yang, J.; Yao, S.; Zhao, K.; Wang, D.; Qin, Q.; Bian, Z.; Li, Y.; Lan, Y.X. Jasmonate signaling enhances RNA silencing and antiviral defense in rice. *Proc. Natl. Acad. Sci. USA* **2020**, *28*, 89–103.
22. Selth, L.A.; Dogra, S.C.; Rasheed, M.S.; Healy, H.; Randles, J.W.; Rezaian, M.A. A NAC domain protein interacts with *Tomato leaf curl virus* replication accessory protein and enhances viral replication. *Plant Cell* **2005**, *17*, 311–325. [[CrossRef](#)] [[PubMed](#)]
23. Huang, Y.; Li, T.; Xu, Z.-S.; Wang, F.; Xiong, A.-S. Six NAC transcription factors involved in response to TYLCV infection in resistant and susceptible tomato cultivars. *Plant Physiol. Biochem.* **2017**, *120*, 61–74. [[CrossRef](#)] [[PubMed](#)]
24. Sun, D.; Zhang, X.; Zhang, Q.; Ji, X.; Jia, Y.; Wang, H.; Niu, L.; Zhang, Y. Comparative transcriptome profiling uncovers a *Lilium regale* NAC transcription factor, LrNAC35, contributing to defence response against *Cucumber mosaic virus* and *Tobacco mosaic virus*. *Mol. Plant Pathol.* **2019**, *20*, 1662–1681. [[CrossRef](#)]
25. Yang, Y.; Klessig, D.F. Isolation and characterization of a *Tobacco mosaic virus*-inducible myb oncogene homolog from tobacco. *Proc. Natl. Acad. Sci. UAS* **1996**, *93*, 14972–14977. [[CrossRef](#)]
26. Li, T.; Zhang, X.Y.; Huang, Y.; Xu, Z.S.; Wang, F.; Xiong, A.S. An R2R3-MYB transcription factor, SlMYB28, involved in the regulation of TYLCV infection in tomato. *Sci. Hortic.* **2018**, *237*, 192–200. [[CrossRef](#)]
27. Huang, Y.; Zhang, B.L.; Sun, S.; Xing, G.M.; Wang, F.; Li, M.Y.; Tian, Y.S.; Xiong, A.S. AP2/ERF transcription factors involved in response to *Tomato yellow leaf curly virus* in tomato. *Plant Genome* **2016**, *9*, plantgenome2015.09.0082. [[CrossRef](#)]
28. Park, C.J.; Shin, Y.C.; Lee, B.J.; Kim, K.J.; Kim, J.K.; Paek, K.H. A hot pepper gene encoding WRKY transcription factor is induced during hypersensitive response to *Tobacco mosaic virus* and *Xanthomonas campestris*. *Planta* **2006**, *223*, 168–179. [[CrossRef](#)]
29. Gaguancela, O.A.; Zúñiga, L.P.; Arias, A.V.; Halterman, D.; Flores, F.J.; Johansen, I.E.; Wang, A.; Yamaji, Y.; Verchot, J. The IRE1/bZIP60 pathway and bax inhibitor 1 suppress systemic accumulation of potyviruses and potexviruses in *Arabidopsis* and *Nicotiana benthamiana* plants. *Mol. Plant-Microbe Interact.* **2016**, *29*, 750–766. [[CrossRef](#)]
30. Gayral, M.; Arias Gaguancela, O.; Vasquez, E.; Herath, V.; Flores, F.J.; Dickman, M.B.; Verchot, J. Multiple ER-to-nucleus stress signaling pathways are activated during *Plantago asiatica mosaic virus* and *Turnip mosaic virus* infection in *Arabidopsis thaliana*. *Plant J.* **2020**, *103*, 1233–1245. [[CrossRef](#)]
31. Meng, X.; Li, G.; Gu, L.; Sun, Y.; Li, Z.; Liu, J.; Wu, X.; Dong, T.; Zhu, M. Comparative metabolomic and transcriptome analysis reveal distinct flavonoid biosynthesis regulation between petals of white and purple *Phalaenopsis amabilis*. *J. Plant Growth Regul.* **2020**, *39*, 823–840. [[CrossRef](#)]
32. Zettler, F.; Ko, N.; Wisler, G.; Elliott, M.; Wong, S. Viruses of orchids and their control. *Plant Dis.* **1990**, *74*, 621–626. [[CrossRef](#)]
33. Kuo, S.Y.; Hu, C.C.; Huang, Y.W.; Lee, C.W.; Luo, M.J.; Tu, C.W.; Lee, S.C.; Lin, N.S.; Hsu, Y.H. Argonaute 5 family proteins play crucial roles in the defence against *Cymbidium mosaic virus* and *Odontoglossum ringspot virus* in *Phalaenopsis aphrodite* subsp. *formosana*. *Mol. Plant Pathol.* **2021**, *22*, 627–643. [[CrossRef](#)]
34. Chao, Y.T.; Yen, S.H.; Yeh, J.H.; Chen, W.C.; Shih, M.C. Orchidstra 2.0—a transcriptomics resource for the orchid family. *Plant Cell Physiol.* **2017**, *58*, e9. [[CrossRef](#)] [[PubMed](#)]
35. Huang, Y.W.; Chang, C.Y.; Hsu, Y.H. Virus-induced gene silencing in Poaceae using a *Foxtail mosaic virus* vector. In *Virus-Induced Gene Silencing in Plants*; Springer: New York, NY, USA, 2020; pp. 15–25.
36. Bazzini, A.A.; Almasia, N.I.; Manacorda, C.A.; Mongelli, V.C.; Conti, G.; Maroniche, G.A.; Rodriguez, M.C.; Distéfano, A.J.; Hopp, H.E.; Del Vas, M. Virus infection elevates transcriptional activity of miR164a promoter in plants. *BMC Plant Biol.* **2009**, *9*, 152. [[CrossRef](#)]

37. Petchthai, U.; Yee, C.S.L.; Wong, S.M. Resistance to CymMV and ORSV in artificial microRNA transgenic *Nicotiana benthamiana* plants. *Sci. Rep.* **2018**, *8*, 9958. [[CrossRef](#)]
38. Li, L.; Yu, X.; Thompson, A.; Guo, M.; Shigeo Yoshida, S.; Tadao Asami, T.; Chory, J.; Yanhai Yin, Y. *Arabidopsis* MYB30 is a direct target of BES1 and cooperates with BES1 to regulate brassinosteroid-induced gene expression. *Plant J.* **2009**, *58*, 275–286. [[CrossRef](#)]
39. Ambawat, S.; Sharma, P.; Yadav, N.R.; Yadav, R.C. MYB transcription factor genes as regulators for plant responses: An overview. *Physiol. Mol. Biol. Plants* **2013**, *19*, 307–321. [[CrossRef](#)]
40. Mabuchi, K.; Maki, H.; Itaya, T.; Suzuki, T.; Nomoto, M.; Sakaoka, S.; Morikami, A.; Higashiyama, T.; Tada, Y.; Busch, W. MYB30 links ROS signaling, root cell elongation, and plant immune responses. *Proc. Natl. Acad. Sci. USA* **2018**, *115*, E4710–E4719. [[CrossRef](#)]
41. Zhang, Y.L.; Zhang, C.L.; Wang, G.L.; Wang, Y.X.; Qi, C.H.; Zhao, Q.; You, C.X.; Li, Y.Y.; Hao, Y.J. The R2R3 MYB transcription factor MdMYB30 modulates plant resistance against pathogens by regulating cuticular wax biosynthesis. *BMC Plant Biol.* **2019**, *19*, 362. [[CrossRef](#)]
42. Fichman, Y.; Zandalinas, S.I.; Sengupta, S.; Burks, D.; Myers, R.J., Jr.; Azad, R.K.; Mittler, R. MYB30 orchestrates systemic reactive oxygen signaling and plant acclimation. *Plant Physiol.* **2020**, *184*, 666–675. [[CrossRef](#)] [[PubMed](#)]
43. Geri, C.; Cecchini, E.; Giannakou, M.E.; Covey, S.N.; Milner, J. Altered patterns of gene expression in *Arabidopsis* elicited by cauliflower mosaic virus (CaMV) infection and by a CaMV gene VI transgene. *Mol. Plant-Microbe Interact.* **1999**, *12*, 377–384. [[CrossRef](#)] [[PubMed](#)]
44. Zhao, S.; Li, Y. Current understanding of the interplays between host hormones and plant viral infections. *PLoS Pathog.* **2021**, *17*, e1009242. [[CrossRef](#)] [[PubMed](#)]
45. Ndamukong, I.; Abdallat, A.A.; Thurow, C.; Fode, B.; Zander, M.; Weigel, R.; Gatz, C. SA-inducible *Arabidopsis* glutaredoxin interacts with TGA factors and suppresses JA-responsive PDF1.2 transcription. *Plant J.* **2007**, *50*, 128–139. [[CrossRef](#)] [[PubMed](#)]
46. Koornneef, A.; Pieterse, C.M. Cross talk in defense signaling. *Plant Physiol.* **2008**, *146*, 839–844. [[CrossRef](#)]
47. Zhu, F.; Xi, D.-H.; Yuan, S.; Xu, F.; Zhang, D.-W.; Lin, H.-H. Salicylic acid and jasmonic acid are essential for systemic resistance against *Tobacco mosaic virus* in *Nicotiana benthamiana*. *Mol. Plant-Microbe Interact.* **2014**, *27*, 567–577. [[CrossRef](#)]
48. He, Y.; Zhang, H.; Sun, Z.; Li, J.; Hong, G.; Zhu, Q.; Zhou, X.; MacFarlane, S.; Yan, F.; Chen, J. Jasmonic acid-mediated defense suppresses brassinosteroid-mediated susceptibility to *Rice black streaked dwarf virus* infection in rice. *New Phytol.* **2017**, *214*, 388–399. [[CrossRef](#)]
49. He, L.; Chen, X.; Yang, J.; Zhang, T.; Li, J.; Zhang, S.; Zhong, K.; Zhang, H.; Chen, J.; Yang, J. *Rice black-streaked dwarf virus*-encoded P5-1 regulates the ubiquitination activity of SCF E3 ligases and inhibits jasmonate signaling to benefit its infection in rice. *New Phytol.* **2020**, *225*, 896–912. [[CrossRef](#)]
50. Siegel, C.S.; Stevenson, F.O.; Zimmer, E.A. Evaluation and comparison of FTA card and CTAB DNA extraction methods for non-agricultural taxa. *Appl. Plant Sci.* **2017**, *5*, 1600109. [[CrossRef](#)]
51. Lescot, M.; Déhais, P.; Thijs, G.; Marchal, K.; Moreau, Y.; Van de Peer, Y.; Rouzé, P.; Rombauts, S. PlantCARE, a database of plant cis-acting regulatory elements and a portal to tools for in silico analysis of promoter sequences. *Nucleic Acids Res.* **2002**, *30*, 325–327. [[CrossRef](#)]
52. Kotnik, T. Lightning-triggered electroporation and electrofusion as possible contributors to natural horizontal gene transfer. *Phys. Life Rev.* **2013**, *10*, 351–370. [[CrossRef](#)] [[PubMed](#)]
53. Horsch, R.; Rogers, S.; Fraley, R. *Transgenic Plants*; Cold Spring Harbor Symposia on Quantitative Biology; Cold Spring Harbor Laboratory Press: Cold Spring Harbor, NY, USA, 1985; pp. 433–437.
54. Van Tunen, A.J.; Hartman, S.A.; Mur, L.A.; Mol, J.N. Regulation of chalcone flavanone isomerase (CHI) gene expression in *Petunia hybrida*: The use of alternative promoters in corolla, anthers and pollen. *Plant Mol. Biol.* **1989**, *12*, 539–551. [[CrossRef](#)] [[PubMed](#)]
55. Clough, S.J.; Bent, A.F. Floral dip: A simplified method for *Agrobacterium*-mediated transformation of *Arabidopsis thaliana*. *Plant J.* **1998**, *16*, 735–743. [[CrossRef](#)] [[PubMed](#)]
56. Liou, M.R.; Huang, Y.W.; Hu, C.C.; Lin, N.S.; Hsu, Y.H. A dual gene-silencing vector system for monocot and dicot plants. *Plant Biotechnol. J.* **2014**, *12*, 330–343. [[CrossRef](#)] [[PubMed](#)]
57. Huang, Y.W.; Hu, C.C.; Liou, M.R.; Chang, B.Y.; Tsai, C.H.; Meng, M.; Lin, N.S.; Hsu, Y.H. Hsp90 interacts specifically with viral RNA and differentially regulates replication initiation of Bamboo mosaic virus and associated satellite RNA. *PLoS Pathog.* **2012**, *8*, e1002726. [[CrossRef](#)]
58. Prasanth, K.R.; Huang, Y.-W.; Liou, M.R.; Wang, R.Y.L.; Hu, C.C.; Tsai, C.H.; Meng, M.; Lin, N.S.; Hsu, Y.H. Glyceraldehyde 3-phosphate dehydrogenase negatively regulates the replication of Bamboo mosaic virus and its associated satellite RNA. *J. Virol.* **2011**, *85*, 8829–8840. [[CrossRef](#)]
59. Cheng, S.F.; Huang, Y.P.; Chen, L.H.; Hsu, Y.H.; Tsai, C.H. Chloroplast phosphoglycerate kinase is involved in the targeting of *Bamboo mosaic virus* to chloroplasts in *Nicotiana benthamiana* plants. *Plant Physiol.* **2013**, *163*, 1598–1608. [[CrossRef](#)]
60. Jefferson, R.A.; Kavanagh, T.A.; Bevan, M.W. GUS fusions: Beta-glucuronidase as a sensitive and versatile gene fusion marker in higher plants. *EMBO J.* **1987**, *6*, 3901–3907. [[CrossRef](#)]
61. Chow, C.N.; Lee, T.Y.; Hung, Y.C.; Li, G.Z.; Tseng, K.C.; Liu, Y.H.; Kuo, P.L.; Zheng, H.Q.; Chang, W.C. PlantPAN3.0: A new and updated resource for reconstructing transcriptional regulatory networks from ChIP-seq experiments in plants. *Nucleic Acids Res.* **2019**, *47*, D1155–D1163. [[CrossRef](#)]

62. Ratcliff, F.; Martin-Hernandez, A.M.; Baulcombe, D.C. Technical advance: Tobacco rattle virus as a vector for analysis of gene function by silencing. *Plant J.* **2001**, *25*, 237–245. [[CrossRef](#)]
63. Livak, K.J.; Schmittgen, T.D. Analysis of relative gene expression data using real-time quantitative PCR and the $2^{-\Delta\Delta CT}$ method. *Methods* **2001**, *25*, 402–408. [[CrossRef](#)] [[PubMed](#)]
64. Pan, X.; Welti, R.; Wang, X. Quantitative analysis of major plant hormones in crude plant extracts by high-performance liquid chromatography–mass spectrometry. *Nat. Protoc.* **2010**, *5*, 986–992. [[CrossRef](#)] [[PubMed](#)]